

# **DEVELOPMENT OF BIOCIDES-CONTAINING CATHETERS FOR CONTROL OF MICROBIAL COLONISATION**

**DEMI TANG**

A thesis submitted in fulfilment of the requirements of Manchester Metropolitan University for the degree of Master of Science (by Research).

**2019**

**Department of Natural Sciences  
Manchester Metropolitan University**

## **ACKNOWLEDGEMENTS**

I would like to express my gratitude to the supervisory team, particularly Dr. Lubomira Tosheva, for her patience, guidance and expertise, Dr. James Redfern, for his support, assistance and encouragement and Dr. Chris Liauw, for his help, insight and scientific advice throughout this project.

I am also grateful for the help of all technical staff involved, especially Dr. Gary Miller and Hayley Andrews for their time, training and help with the analysis of samples.

Furthermore, I'd like to thank Mike Green for his cheery instruction, Greg Woodhead for constantly boosting morale and David McKendry for his insight into ICP.

Ultimately, I must give thanks to my friends, colleagues and family, all of whom have helped keep me sane this past year. I truly appreciate their support.

## ABSTRACT

Catheter-associated urinary tract infections (CAUTIs) are the most common health-care associated infections, which contribute greatly to the morbidity and mortality of critically ill patients. This systematic study investigated metal organic framework (MOF) structures in the forms of Zeolitic Imidazolate Framework-8 (ZIF-8) and ZnO@ZIF-8, regarding the effects of synthesis route on antimicrobial ability and their incorporation into silicone elastomer composites. The conformability (in terms of mechanical properties) of each embedded composite sample was assessed, and comparisons were made against commercial, dermatologically tested maxillofacial silicone.

Two ZIF-8 materials were synthesised in organic and aqueous media, correspondingly, which resulted in crystals of different sizes and morphologies. The ZIF-8 (MeOH) prepared in methanol medium at room temperature resulted in 60 nm spherical nanoparticles. The ZIF-8 (TEA) prepared in aqueous medium in the presence of triethylamine (TEA) at room temperature contained ca. 250 nm cubic crystals. The two samples were post-synthetically treated with silver nitrate to convert into ZnO@ZIF-8 materials, as a result of the spontaneous growth of ZnO nanorods within ZIF-8. Antimicrobial ability was established for all samples with average minimum bactericidal concentrations (MBCs) (mg/mL) in the range 0.0228 – 0.0709. The samples were incorporated into composite silicone samples (4 wt.% of biocide). Introduction of ZnO-nanorods to the structures increased the antimicrobial activity.

Investigations into composite mechanical properties showed that ZnO@ZIF-8 (MeOH) interfered with the curing of silicone polymers most, despite presenting the lowest MBC (mg/mL). With regards to other incorporated ZIFs, mechanical properties of the composite silicones were not detrimentally affected. Successful biocidal action of the MOF-loaded silicones was demonstrated using the microbiology method BS ISO 22196:2011, against the model bacterium, *Escherichia coli*. This study highlighted the significant potential of antimicrobial ZIFs in the development of biocide-containing catheters. Incorporation of ZnO-nanorods in particular, provided promising evidence for the control of microbial colonisation.

## Table of Contents

Acknowledgements.....	2
Abstract.....	3
Contents List.....	4
List of Figures.....	6
List of Tables.....	8
List of Abbreviations.....	9
Chapter 1: Introduction.....	10
1.1. Metal Organic Frameworks.....	11
1.2. Zeolitic Imidazolate Frameworks.....	14
1.3. Antimicrobial Resistance.....	18
1.4. Catheter Associated Urinary Tract Infections.....	19
1.5. Antimicrobial Applications of Metal Organic Frameworks.....	21
1.6. Silicone Polymers for Medical Use.....	23
1.7. Aims and Objectives.....	25
Chapter 2: Experimental.....	26
2.1. Synthesis of ZIF-8 and ZnO@ZIF-8.....	26
2.1.1. Upscaling synthesis.....	27
2.1.2. Calcining products.....	27
2.2. Characterisation of Samples.....	27
2.3. Antimicrobial Testing of ZIF-8 and ZnO@ZIF-8.....	28
2.3.1. Maintenance and standardization of microorganisms.....	28
2.3.2. MBC assay.....	29
2.4. Synthesis of Composite Samples.....	30
2.5. Assessment of ZIF Particle Dispersion Quality.....	30
2.5.1. Macro-dispersion.....	31

2.5.2.	Micro-dispersion from freeze-fracture analysis.....	31
2.6.	Composite Properties.....	31
2.6.1.	Percent mass hexane swelling and extractables.....	31
2.6.2.	Tensile testing.....	32
2.7.	Antimicrobial Testing of Composite Samples.....	33
2.7.1.	Measurement of antibacterial activity on composite samples....	33
2.8.	Metal Release Testing in Artificial Urine.....	34
Chapter 3: Results and Discussion.....		35
3.1.	Synthesis of ZIF-8.....	35
3.1.1.	Synthesis in organic medium.....	35
3.1.2.	Synthesis in aqueous medium.....	36
3.1.3.	Post-synthetic modification of ZIF-8.....	40
3.2.	Antimicrobial Testing of ZIF-8 and ZnO@ZIF-8.....	48
3.2.1.	Minimum bactericidal concentration assay.....	48
3.3.	Silicone elastomers containing ZIF-8 and ZnO@ZIF-8.....	50
3.3.1.	Effect of ZIF-8 and ZnO@ZIF-8 addition on polymer curing.....	50
3.3.2.	Effect of adsorbed gas release on cured polymer structure.....	50
3.3.3.	Macro-dispersion quality.....	51
3.3.4.	Micro-dispersion quality.....	52
3.3.5.	Percent mass hexane swelling and extractables.....	53
3.3.6.	Tensile testing.....	55
3.4.	Antimicrobial Testing of Composite Samples.....	59
3.4.1.	Measurement of antibacterial activity on composite samples....	59
3.5.	Metal release testing in artificial urine.....	60
Chapter 4: Conclusions.....		67
Chapter 5: Future Work.....		68
References.....		70

## LIST OF FIGURES AND TABLES

### List of Figures

**Figure 1:** Chemical structure of ZIF-8. Blue tetrahedra depict zinc-nitrogen bonds, whilst the orange sphere represents ZIF-8's open-pore structure. Image taken from Redfern et al, 2018.

**Figure 2:** Schematic diagram representing the spontaneous local transformation of ZIF-8 into the ZnO@ZIF-8 nanocomposite, embedded with ZnO nanorods. Image reproduced from Redfern et al, 2018.

**Figure 3:** Mechanism showing the oxidative addition of the  $\equiv\text{Si}$  to the Pt, H transfer to the double bond, and reductive elimination of the product. To simplify, other Pt ligands and other Si substituents have been omitted. Image adapted from Colas and Curtis, 2004.

**Figure 4:** XRD patterns of ZIF-8 samples prepared using (a) methanol (MeOH), (b) industrial methylated spirit (IMS) and (c) N, N-Dimethylformamide (DMF).

**Figure 5:** SEM images of ZIF-8 samples prepared with: (a) MeOH, (b) IMS and (c) DMF solvents.

**Figure 6:** XRD patterns of ZIF-8 samples prepared using 1 cm<sup>3</sup> - 4 cm<sup>3</sup> TEA (a-d respectively).

**Figure 7:** SEM images from aqueous ZIF-8 synthesis using (a) 1 cm<sup>3</sup> TEA, (b) 2 cm<sup>3</sup> TEA, (c) 3 cm<sup>3</sup> TEA and (d) 4 cm<sup>3</sup> TEA. Scale bars indicate 200 nm.

**Figure 8:** XRD patterns of ZIF-8 prepared using 3 cm<sup>3</sup> TEA: (bottom) as-made and (top) heat-treated at 200°C.

**Figure 9:** XRD patterns of (a) batch ZIF-8 sample prepared using methanol and (b) the corresponding ZnO@ZIF-8 sample. The asterisk indicates ZnO XRD peaks (reference pattern 96-900-4182).

**Figure 10:** XRD patterns of (a) batch ZIF-8 sample prepared from the TEA system and (b) the corresponding ZnO@ZIF-8 sample.

**Figure 11:** SEM images of ZnO@ZIF-8 samples prepared with: (a) MeOH, (b) 3 cm<sup>3</sup> TEA.

**Figure 12:** EDX spectra of ZnO@ZIF-8 prepared using MeOH.

**Figure 13:** EDX spectra of ZnO@ZIF-8 prepared using TEA.

**Figure 14:** Nitrogen adsorption desorption isotherms at -196°C of (a) ZIF-8 (MeOH) and (b) ZnO@ZIF-8 (MeOH) samples.

**Figure 15:** Nitrogen adsorption desorption isotherms at -196°C of (a) ZIF-8 (TEA) and (b) ZnO@ZIF-8 (TEA) samples.

**Figure 16:** Digital images of cured composite samples containing (A) unfilled matrix, (B) ZIF-8 prepared with MeOH, (C) ZnO@ZIF-8 prepared with MeOH, (D) ZIF-8 prepared with TEA and (E) ZnO@ZIF-8 prepared with TEA.

**Figure 17:** SEM images of freeze-fractured composite samples containing (A) unfilled matrix, (B) ZIF-8 prepared with MeOH, (C) ZnO@ZIF-8 prepared with MeOH, (D) ZIF-8 prepared with TEA and (E) ZnO@ZIF-8 prepared with TEA. Scale bar is 200 nm (A, B and E) and 300 nm (C and D).

**Figure 18:** Average hexane swelling (A) and extractables content (B) (all mass percentages) of ZIF samples and unfilled matrix control.

**Figure 19:** Average stress-strain curves of ZIF samples versus unfilled matrix (Av Str Control).

**Figure 20:** Average percentage elongation at break (A), tensile strength / MPa (B) and Young's Modulus /MPa (C) values of ZIF samples versus unfilled matrix control.

**Figure 21:** Average numbers of colony forming units (living *E. coli*, CFU/mL) recovered from 4 wt.% ZIF composite coupons and unfilled matrix (control), at set time points.

**Figure 22:** XRD patterns of the batch ZIF-8 sample, prepared from the MeOH system: (a) before and (b) after leaching.

**Figure 23:** XRD patterns of the batch ZnO@ZIF-8 sample, prepared from the MeOH system: (a) before and (b) after leaching.

**Figure 24:** XRD patterns of the batch ZIF-8 sample, prepared from the TEA system: (a) before and (b) after leaching.

**Figure 25:** XRD patterns of the batch ZnO@ZIF-8 sample, prepared from the TEA system: (a) before and (b) after leaching.

## List of Tables

**Table 1:** Sample key for materials tested by MBC assays.

**Table 2:** BET surface areas of ZIF-8 from organic and aqueous synthesis routes.

**Table 3:** BET surface areas ( $S_{\text{BET}}$ ), total pore volumes ( $V_{\text{total}}$ ) and micropore volumes ( $V_{\text{micro}}$ ) of the four batch samples prepared.

**Table 4:** Heat-mapped average MBC ( $\text{mgmL}^{-1}$ ) values of samples subjected to minimum bactericidal concentration assays, with sample numbers corresponding to Table 1. Green shows the lowest figures, with progression through amber to red as values increase.

**Table 5:** Concentrations of Zn and Ag detected from ICP analysis of artificial urine, following exposure to composite samples with 85 days incubation.

**Table 6:** Concentrations of Zn and Ag detected from ICP analysis of artificial urine, following exposure to powdered samples with 85 days incubation.

## List of Abbreviations

**Abs. EtOH:** Absolute ethanol

**AMR:** Antimicrobial resistance

**BET:** Brunauer-Emmett-Teller

**CAUTIs:** Catheter associated urinary tract infections

**CIP:** Ciprofloxacin

**CVD:** Chemical Vapour Deposition

**EDX:** Energy-Dispersive X-Ray Spectroscopy

***E. coli:*** *Escherichia coli*

**HIV:** Human immunodeficiency virus

**Hmim:** 2-methylimidazole

**ICP-MS:** Inductively Coupled Plasma Mass Spectrometry

**MBC:** Minimum bactericidal concentration

**MeOH:** Methanol

**MOFs:** Metal-organic frameworks

**NPs:** Nanoparticles

**PDMS:** Polydimethylsiloxane

**PE:** Polyethylene

**PTFE:** Polytetrafluoroethylene

**SALE:** Solvent assisted linker exchange

**SALI:** Solvent assisted linker incorporation

**SEM:** Scanning electron Microscopy

**SOD:** Sodalite

**TB:** Tuberculosis

**TEA:** Triethylamine

**UI:** Urinary incontinence

**UTIs:** Urinary tract infections

**XRD:** X-Ray diffraction

**ZIFs:** Zeolitic imidazolate frameworks

## CHAPTER 1: INTRODUCTION

Catheter-associated urinary tract infections (CAUTIs) are amongst the most common infections acquired in the healthcare environment worldwide.<sup>1, 2</sup> Colonisation of a catheter by a microorganism can result in biofilm, often causing blockages.<sup>3, 4</sup> If microorganisms reach the patient, infections may be caused - some of which are becoming more difficult to treat due to the emergence of antimicrobial resistance.<sup>5, 6</sup> Due to this, the development of catheter materials with the ability to control microbial colonisation is much needed to help reduce the frequency of antibiotic treatments.

Research into porous materials, such as zeolites, ordered mesoporous silicas and metal-organic frameworks (MOFs), has identified structures with large surface areas and uniform pore sizes, enabling the release of antimicrobials and thus the demonstration of antimicrobial activity. Whilst zeolites and ordered mesoporous silicas have shown drawbacks regarding low drug-storage capacity, alongside too rapid drug delivery,<sup>7</sup> MOFs have presented promising characteristics and properties suggesting controlled and sustained effects.<sup>8</sup> Furthermore, tuneable MOF crystal sizes, ranging from the nano- to micro-scale, allow for the variation of both internal and external surface areas. Hydrophobic MOFs are ideal candidates to incorporate into polymers and thus, could permit composite polymer materials to have long-term antimicrobial activity. This study examines the antimicrobial abilities of Zeolitic Imidazolate Framework-8 (ZIF-8), which was not shown to have antimicrobial activity, and of ZnO@ZIF-8 - a highly potent antimicrobial, as demonstrated by preliminary studies.<sup>9</sup> Various sizes of ZIF-8 were prepared and tested prior to post-synthesis treatment to form ZnO@ZIF-8, then embedded into silicone elastomer composite samples.<sup>9</sup> Antibacterial activity of the composite samples was conducted using BS ISO 22196:2011, and mechanical testing ensued to monitor material properties.

The successful development of a biocide-embedded silicone would hold great potential to help eradicate CAUTIs. Should the material be suitable for biocide-containing catheters, the global threat of increased antimicrobial resistance would also be reduced.

## 1.1. Metal Organic Frameworks

Metal-organic frameworks (MOFs) are an exciting class of materials, offering an ever-expanding scope of research. Also known as porous coordination polymers, MOFs are 3D-ordered porous materials, composed of inorganic metal clusters, bridged by organic linkers such as carboxylates, phosphonates, or nitrogen-containing ligands. In certain cases, these structures exhibit record-setting Brunauer-Emmett-Teller (BET) surface areas that can be as high as  $\sim 7000 \text{ m}^2/\text{g}$ , compared to that of up to  $1000 \text{ m}^2/\text{g}$  for zeolites, making them exceedingly favourable for their potential applications.<sup>10, 11</sup> The ultrahigh porosity of MOFs (up to 90% free volume), has been unsurpassed by any other material,<sup>12</sup> and it has been demonstrated computationally that MOF materials may have hypothetical surface areas as high as  $\sim 14600 \text{ m}^2/\text{g}$ .<sup>10</sup> The discovery of these properties stems from a vast number of research papers published within the last thirty years, which highlight their importance and depict intriguing crystalline material advances.<sup>12-16</sup> Fundamentally, structures of MOFs combine organic with inorganic chemistry, interlinking contrasting disciplines and creating a plethora of topologically diverse and flexible structures. By appropriately selecting their organic and inorganic components, MOFs can be tailored for purpose, e.g. they may have one, two or three dimensional structures, incorporating micro- or meso-sized pores.<sup>17</sup> Such structures may be formed with or without open metal centers, and have the ability to append functional groups within their pores.<sup>18</sup> Nanoscale MOFs in particular exhibit unique physical and chemical properties, distinctly due to their corresponding bulk materials.<sup>19, 20</sup> The design of MOF-derived nano-structures has led to a recognition of the importance of morphology in the enhancement of MOF performance.<sup>21</sup> When compared to their components alone, such structures display a broader range of external surface areas, shapes (tunnels, cages, etc.) and abilities.<sup>22, 23</sup>

The design of target MOFs with specific properties and functions has become a boundless aspiration for scientists from a variety of backgrounds. Resultantly, MOF synthesis has developed a plethora of different synthetic methods and strategies, though typically follows a solution-mediated reaction process.<sup>24, 25</sup> Despite starting from the same reaction mixtures, divergent metal organic frameworks can be obtained by applying a variety of routes and conditions.<sup>26</sup> Depending upon the intended application of MOFs, careful thought must be given to the preferred

reaction time, yield, temperatures, particle sizes and morphologies - particularly if the intention is to mass-produce the MOF on a large scale. Synthesis routes range from conventional to systematic, whilst computational and alternative routes are in continuous development, e.g. microwave-assisted,<sup>27</sup> electrochemical,<sup>28</sup> mechanochemical<sup>29</sup> and sonochemical syntheses.<sup>30</sup>

Conventional MOF synthesis refers to reactions which require conventional electric heating, without parallelisation of reactions. It may be refined to two routes; solvothermal and non-solvothermal synthesis.<sup>24</sup> In most cases, solvothermal synthesis refers to reactions occurring under autogenous pressure, above the boiling point of the chosen solvent, within a closed vessel.<sup>31</sup> Non-solvothermal synthesis however, refers to reactions occurring at or below the boiling point of the solvent, under ambient pressure.

In contrast, non-conventional MOF synthesis can entail solvent evaporation of a solution of reactants, the layering of solutions, and the slow diffusion of reactants into each other. Drawbacks exist when using these approaches for commercial, large-scale synthesis and harmful and environmentally hazardous organic solvents are regularly required. High temperatures and long reaction times are often necessitated. Where sealed and pressurised reaction vessels are concerned, high processing costs become inevitable.<sup>32</sup>

The expertise of those researching MOFs has been a driving force for alternative method development. Coordination chemistry has accounted for the introduction of electrochemical and mechanochemical syntheses, as well as concepts like the precursor approach or in situ linker synthesis. First reported in 2005, electrochemical MOF synthesis permits a continuous process with the possibility of obtaining a higher solids content than those gained from batch reactions.<sup>24</sup> It has become favourable for industrial processes, although H<sub>2</sub> is regularly formed as a by-product. Mechanochemical synthesis techniques have also advanced, whereby reactions require the mechanical breakage of intramolecular bonds to permit a chemical transformation. Initially described in 2006, this route became environmentally favourable due to the exclusion of organic solvents.<sup>33</sup> With this, metal oxides can be replaced by metal salts, and water remains as the only side-product. The process generally produces MOFs of small particle sizes, requires short reaction times and provides quantitative yields – thus, interest surrounding mechanically activated MOF synthesis has grown rapidly.

Furthermore, organic chemistry has been responsible for microwave-assisted MOF synthesis. Microwave-heating is a well-known energy source, which results in fast reaction rates and short reaction times. Due to quick kinetics of crystal nucleation and growth, high product yields of good phase purity, and few or no secondary products, such routes are also favourable.<sup>34</sup> MOFs, such as MOF-5 and IR-MOF1, have been well-characterized this way and large quantities of such frameworks are successfully isolated over economically-viable periods of time.<sup>27, 35</sup> Much focus in this field has surrounded the development of nano-sized crystallites, which are particularly useful in functional devices.

For most MOF syntheses, reactions occur in the presence of a solvent at temperatures ranging from ambient to ~250°C. Heat and energy can be generated by multiple means leading to further alternative synthesis routes. These may utilise electric potential, electromagnetic radiation, mechanical waves (ultrasound), or mechanical methods of energy input.<sup>36</sup> The duration, pressure and energy per molecule within the system is directly related to the energy source provided, which in turn influences the formation of the product, particle size, size distribution and particle morphology.

Consequentially, the MOFs' properties and suitability to applications may be affected, i.e. there may be a direct impact on catalytic reactions or the adsorption and separation of molecules. Today, MOFs are almost routinely designable to withstand severe physical and chemical conditions. MOFs with particularly strong stabilities are often used as heterogeneous catalysts in chemically harsh, condensed phases, as well as in thermally challenging conditions relevant to gas-phase reactions.<sup>18</sup> Industrial applications, such as moderate-temperature storage,<sup>37</sup> ion exchange<sup>38</sup> and gas separation<sup>39</sup> rely on chemical (specifically hydrolytic) and thermal stabilities. Favoured, compacted MOF forms (such as pellets) are also required to be mechanically stable.<sup>40</sup> Modern advances have led to frameworks with varied combinations of mechanical, thermal and chemical stabilities. However, no single MOF with perfect stability in all fields currently exists.

Applications of MOFs have mostly focused on clean-energy and environmental protection. Much published research is based on catalysis, gas storage, separation and carbon-capture, however contemporary advances have been made regarding their integration with electronic devices and chemical sensors.<sup>41-47</sup> The literature also describes MOFs in the removal of toxic industrial chemicals and chemical

warfare agents.<sup>48, 49</sup> In closer relation to this study, advancements have been reported in biological and medicinal MOF applications (e.g. biomolecule encapsulation and drug delivery).<sup>50-52</sup> These are of particular interest when considering the development of MOFs with antimicrobial ability.<sup>7, 53, 54</sup> Overall, the ultimate aim is to find a fast, energy-efficient and environmentally-friendly, room temperature method, that can easily be carried out on a mass scale for the formation of any MOF structure desired.

## **1.2. Zeolitic Imidazolate Frameworks**

Zeolitic imidazolate frameworks (ZIFs) are a tetrahedrally-coordinated subclass of MOFs, consisting of a divalent metal cation and four imidazolate anion ligands.<sup>55</sup> Composed via self-assembly, metal ions such as  $Zn^{2+}$  are linked through the nitrogen atoms of deprotonated frameworks.<sup>56</sup> They possess topologies analogous to zeolite structures and are most easily illustrated by their sodalite-type cages.<sup>57, 58</sup> Like MOFs, ZIFs have tunable pore sizes and versatile functionalities, though typically exhibit greater chemical and thermal stabilities than traditional MOFs alone.<sup>59</sup> This is likely due to increased basicity from the imidazolate-type linkers, which depending upon their position and bulkiness, may result in the synthesis of ZIFs with distinct and different topologies.<sup>60</sup> Such topologies often show similarities to those of inorganic zeolites,<sup>61</sup> i.e. rhodolite (RHO), sodalite (SOD), gmelinite (GME), and Linde type A (LTA).<sup>62</sup>

Whilst tuning the functional properties and pore structures of ZIFs, numerous novel ZIF topologies and compositions have been developed. These are suitable for uses in gas storage, gas separation and catalysis.<sup>62</sup> In chemical separations, ZIFs have been favoured over the use of zeolites. Milder synthesis conditions are required and customisable frameworks allow them to be competitive candidates for the production of high-quality membranes.<sup>63</sup> These extensively explored ZIF membranes and adsorbents have consequentially emerged as a new family of molecular sieves and porous structures; particularly useful in controlled drug delivery systems (DDS)<sup>64</sup> and energy-efficient separation technologies. Thus, investigations are now focused on more reliable and scalable ZIF manufacture.<sup>65</sup> Alongside crystalline ZIFs, amorphous ZIFs have been obtained from their crystalline counterparts through heating,<sup>66</sup> pressurising,<sup>67</sup> ball-milling<sup>68</sup> and electrical discharge procedures.<sup>69</sup> Such structures have also been explored for applications in guest

immobilization and drug delivery.<sup>58</sup> Due to their distinct, yet similar, structure to the parent ZIF, these amorphous frameworks may provide a platform to complement thin film membrane, sensor and low-*k* dielectric devices.<sup>58, 70</sup> Currently, the most extensively studied ZIF is ZIF-8 (**Fig. 1**).

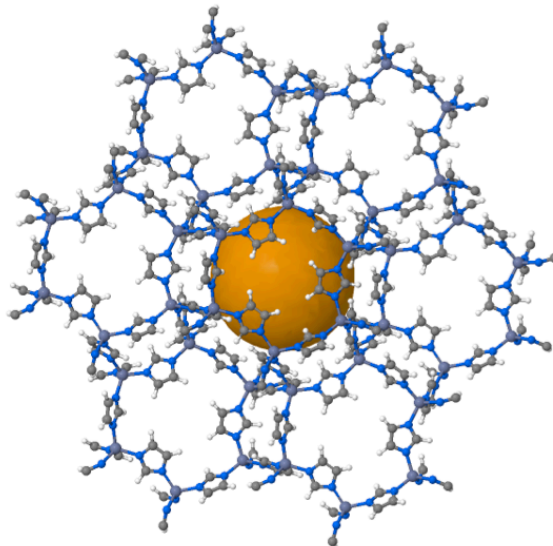


**Figure 1: Chemical structure of ZIF-8. Blue tetrahedra depict zinc-nitrogen bonds, whilst the orange sphere represents ZIF-8's open-pore structure. Image taken from Redfern et al, 2018.<sup>9</sup>**

Formed from zinc ions tetrahedrally coordinated to 2-methylimidazole (Hmim), ZIF-8 has gained considerable attention due to its high surface area, and high thermal (>550°C under N<sub>2</sub>), mechanical and chemical stabilities.<sup>60, 71</sup> It exists as a SOD topology, which crystallises in a cubic lattice (space group *I43m*) with a lattice constant of 16.992 Å. ZIF-8 houses great flexibility, with pore cavities of 11.6 Å accessible through theoretical pore apertures of ~3.4 Å.<sup>72</sup> Due to the 'flip-flopping' motion of ZIF-8's linkers however, said frameworks realistically possess an effective aperture size of ~4.0 Å.<sup>73</sup>

The material applications of ZIF-8 lie in membrane-based gas separation, carbon dioxide capture, hydrogen storage, small molecule separation, catalysis, drug delivery,<sup>74-77</sup> and as a cathode material for lithium-sulphur batteries (S@ZIF-8).<sup>78</sup> Literature has recently described ZIF-8 to show biocompatibility and non-toxicity.<sup>79</sup> During investigations, its use as a potential drug vehicle for cancer treatments showed acid responsiveness and moderate biocompatibility.<sup>60, 80, 81</sup>

Typically, solvothermal processes are used to form ZIFs, which require the mixture of a highly diluted metal salt with organic ligands, within an organic solvent. An autoclave then heats this mixture to temperatures up to 200°C.<sup>60, 71, 82, 83</sup> Though

ZIF-8 is usually prepared by similar methods, recent publications have described more environmentally-friendly, non-solvothermal and aqueous routes. These methods are significantly quicker and require much less energy consumption.<sup>84-87</sup> Microporous ZIF-8 has also been prepared by various means of solvothermal syntheses,<sup>60</sup> chemical vapour deposition (CVD),<sup>88</sup> and steam-assisted conversion.<sup>89</sup> Adaptations of both organic and aqueous synthesis routes were used in this study to rapidly form ZIF-8 nanoparticles of different sizes. Both colloidal chemistry routes were conducted at room temperature, resulting in lowered energy consumption when compared to the most common solvothermal methods.<sup>87, 90</sup>

Now vastly cited, Cravillon et al. became the first to report on the characterisation and synthesis of a nanoscale ZIF-8 material.<sup>90</sup> This organic route relies upon the combination of a methanol solution of  $\text{Zn}(\text{NO}_3)_2 \cdot 6\text{H}_2\text{O}$ , into a methanol solution of 2-methylimidazole (Hmim) at room temperature. An approximate ratio of 1:8:700, of  $\text{Zn}(\text{NO}_3)_2 \cdot 6\text{H}_2\text{O}$ , Hmim, and MeOH is required respectively. The resultant ZIF-8 did not require any activation or auxiliary stabilisation, and good yields of single-phase, rhombic dodecahedron, ZIF-8 nanocrystals were obtained.<sup>90</sup> This fast, non-solvothermal method required much less time and energy than alternative syntheses, offering a favourable route for achieving good product yields.

By further refining the environmental effects of ZIF-8 production, successful aqueous synthesis routes have developed.<sup>84, 85, 87</sup> Investigations have focused on the resultant ZIF-8's crystallinity, particle size and morphology.<sup>87</sup> Nordin et al., in particular, have built upon an existing aqueous synthesis route, which also resulted in rhombic dodecahedron nanocrystals. This method refined previously detailed chemical usage and increased the ZIF-8 yield, prior to investigating the control of ZIF-8 particle size.<sup>85, 87</sup> A molar ratio of 1:6:500 of  $\text{Zn}(\text{NO}_3)_2 \cdot 6\text{H}_2\text{O}$ :Hmim: $\text{H}_2\text{O}$  was chosen, with ratios of triethylamine (TEA) added to the Hmim solution, relative to the total molar amount of the synthesis solution. The ZIF-8 product was collected after 30 minutes via centrifugation, and then washed with deionized water prior to drying.<sup>87</sup> Yields of 85% resulted, following the removal of any impure components. By altering the ratio of TEA, ZIF-8 particle size could be controlled. Adapting this method allowed nanocrystalline ZIF-8 (of particle sizes different to those gained from organic means), to be obtained and investigated. Although well-documented, electrochemical, mechanochemical and microwave-assisted synthesis routes for ZIF-8, were not used within this study.

Properties of MOFs (and thus ZIFs), can be enhanced or altered by means of post-synthetic modification (PSM). This requires the modification or exchange of the metal ion and/or the organic linker of the framework, following synthesis. Ligand molecules may be post-synthetically replaced and other linkers may be incorporated into MOFs using routes known as solvent assisted linker exchange (SALE) or solvent assisted linker incorporation (SALI).<sup>91-93</sup> Modifications may be covalent and/or dative, and are responsible for many recent advances within the MOF field. One significant example is the use of MOFs for the adsorption and release of drugs. Here, the biodegradable character within the ZIF can be modified by the choice of the metal, organic linker and structure.<sup>12</sup>

With regards to ZIF-8, PSM has resulted in frameworks with enhanced capabilities. Mesopores can be introduced to the framework and thus promote mass transfer kinetics within the ZIF-8 structure. Due to this, the size and diffusion limits of the original ZIF-8's micropores are exceeded.<sup>78, 94</sup>

More pertinent to this study are the works by Wee et al. and Yang et. al., whom both use solutions of silver nitrate for the formation of ZnO@ZIF-8 from pure-phase ZIF-8 samples.<sup>95, 96</sup> This PSM of ZIF-8, conductively generates fixed ZnO nanorods within the ZIF-8 matrix (**Fig. 2**). It is a spontaneous room temperature transformation, which requires the suspension of ZIF-8 nanopowder in a silver nitrate solution of 53.7 mM  $\text{AgNO}_3$ , made with a 1:6, water:ethanol solution. This light-sensitive mixture is then covered and agitated overnight, prior to removing the product by centrifugation.

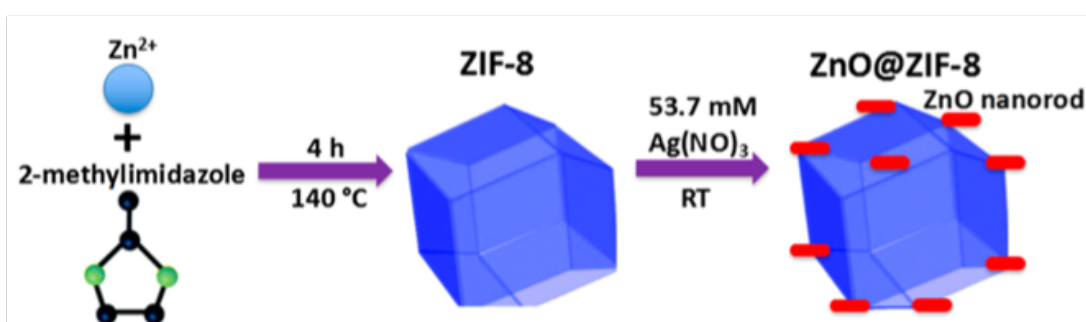


**Figure 2: Schematic diagram representing the spontaneous local transformation of ZIF-8 into the ZnO@ZIF-8 nanocomposite, embedded with ZnO nanorods. Image reproduced from Redfern et al, 2018.<sup>9</sup>**

The resultant ZnO@ZIF-8 must be washed with absolute ethanol and dried at ambient temperature.<sup>95</sup> ZnO nanorods are particularly well-known for their antimicrobial properties.<sup>97-99</sup>

### 1.3. Antimicrobial Resistance

Throughout the past decade, the presence, growth and effects of antimicrobial resistance (AMR) have been comprehensively documented worldwide.<sup>100</sup>

Referring to those active against a range of pathogens, i.e. bacteria (antibiotics), viruses (antivirals), fungi (antifungals) and parasites (e.g. antimalarials) - antimicrobial drugs have allowed huge advances in both public health and global agriculture.<sup>101-103</sup>

Although resistance to antimicrobials is a natural occurrence,<sup>104</sup> overuse of such drugs has caused the rate of resistance development and its affected scope to increase.<sup>105</sup> As a result, the fight against life-threatening infectious diseases and the availability of antimicrobial prophylaxis is at risk of significant regression. Furthermore, AMR has vast economic impact. In the United States (US) alone, over two million infections per year are caused by pathogens resistant to their first-line antimicrobial treatments, costing the US health system 20 billion USD.<sup>106</sup>

Undoubtedly, drug-resistant infections are claiming lives. Each year, ~700,000 fatalities are reported globally due to AMR strains of common bacterial infections, tuberculosis (TB), human immunodeficiency virus (HIV) and malaria.<sup>105</sup> This includes deaths reported of patients contracting secondary bacterial infections, e.g. from *Klebsiella pneumoniae* in HIV patients, *Escherichia coli* (*E. coli*) in TB patients and *Staphylococcus aureus* in those with malaria.<sup>100</sup> 'Last-resort' treatments known to cause severe side effects are now being used more readily. In the case of the antibiotic colistin, for example, previous prescription was avoided due to associated kidney toxicity.<sup>105</sup> The drug has since re-emerged as a last-resort against Gram-negative bacteria already showing resistance to other drugs. Unfortunately however, colistin-resistance has recently been reported in Gram-negative bacilli infections and in these cases, alternative antibiotic treatments are not currently available.<sup>107</sup>

#### **1.4. Catheter Associated Urinary Tract Infections**

Catheter-associated urinary tract infections (CAUTIs) are the second most common cause of hospital-acquired infections worldwide.<sup>108</sup> As the most preventable form of health-care associated infection, they cause avoidable morbidity and increased health-care costs throughout developing and high-income countries.<sup>109, 110</sup> Despite this, antibiotic prophylaxis of asymptomatic CAUTIs is not recommended, as this may increase the rate of AMR without eradicating pathogenic bacteria. Most commonly used in 'at risk' persons, i.e. hospitalised and post-operative patients, and those with urinary incontinence (UI) - most frequently shown in the elderly population, urethral catheters are regularly positioned long-term.<sup>111</sup> It was reported in 1997, that 100% of patients developed a bacterial urinary tract infection within 30 days of long-term catheterisation.<sup>112</sup> This was reflected by an estimated total cost to the UK's National Health Service of £1.4 billion each year, in UI treatment alone.<sup>111, 113</sup>

Urethral catheters have been used for more than 3500 years, allowing the drainage of urine on an intermittent or indwelling basis.<sup>114</sup> Though developed significantly throughout the 20<sup>th</sup> Century, little modification has been made since the introduction of the 'closed' catheter system in the 1960s.<sup>115</sup> With this, urine is drained through a tube and into a fused receptacle. A contained environment for the urine results, protecting it from the contaminated environment. The space between the external catheter and the urethral mucosa, however, offers the opportunity for direct pathogenic entry to the bladder. This is the most common route of bacterial entry.<sup>116</sup> Bacteria such as *Proteus mirabilis* are urease-producing. When present, urase hydrolyses urea and generates ammonia, which increases the pH of the urine and leads to the formation of hydroxyapatite and struvite crystals. As these crystals grow, the catheter becomes coated by the crystalline deposits, allowing bacteria to attach and multiply. This often limits the efficacy of antimicrobial coatings, since contact with the underlying protective coating is reduced.<sup>117</sup> Within 24 hours, bacteria present in the catheterised urinary tract are able to multiply to high concentrations.<sup>118</sup> Biofilm growth on both the inner and outer catheter surfaces is common, especially if crystal-coated. This entails the cultivation of a structured community of microorganisms, which then becomes encapsulated within a self-developed polymeric matrix.<sup>117</sup> The biofilm adheres to the catheter lumen, becoming incredibly difficult to eradicate since antibacterial agents are often unable to

penetrate the biofilm's full depth.<sup>4, 119</sup> Once symptomatic CAUTIs are shown, systemic antibiotics are employed, bacterial resistance increases in cases of biofilm formation however, and often secondary ailments arise requiring further treatments, e.g. chronic bacterial prostatitis.<sup>117</sup>

Thus, the development of antimicrobial catheter materials with the ability to control microbial colonisation would be greatly beneficial. Current practice recommends treating only symptomatic CAUTIs with antibiotics, unless cases of pregnancy, pre-urological surgery, or patients with high risks of serious infectious complications with strains causing a high incidence of bacteraemia (e.g. *Serratia marcescens*, *Escherichia coli* and *Proteus mirabilis*), are shown.<sup>120, 121</sup>

A variety of efforts to modify catheter materials and/or their surface properties have been made. The hope is to prevent or effectively delay biofilm formation and thus prevent, or delay, the onset of CAUTIs.

Silver alloy-coated latex catheters and nitrofurantoin-impregnated silicone catheters have indicated the inhibition of urinary pathogens.<sup>122</sup> However, despite their ability to reduce the bacterial contamination of urine, their actual usefulness against symptomatic CAUTI was uncertain.<sup>123</sup> It has also been concluded that CAUTI incidence is greater in male catheter users, but that infection is more frequent when latex materials are positioned in place of silicone ones.<sup>124</sup>

Research into surface modifications to alter hydrophobicity and the creation of antiadhesive surfaces (e.g. heparin and phosphorylcholine), has also been made.<sup>120</sup> Unfortunately, their long-term efficacy could not be proven.<sup>117</sup>

The development of an antimicrobial agent effective against bacteria in CAUTI-causing biofilms is an ultimate goal and an optimal catheter material or coating is still awaited. Benefits of such an accomplishment would not only positively affect the economy and healthcare sector, but also aid the patients concerned. At present, the most effective methods of CAUTI prevention are to avoid unnecessary catheterisation and to remove catheters as soon as possible.<sup>120</sup>

## 1.5. Antimicrobial Applications of Metal Organic Frameworks

Research into the antimicrobial applications of metal organic frameworks remains in its infancy. Due to their highly functional and tailorable make-ups, antimicrobial properties may result from the MOF's composition, structure and/or its vast internal volumes. When considering a MOF's organic linkers, ligands may be chosen which are biologically active and/or already known to display antimicrobial activity. Reservoirs within the framework can also provide spaces in which guest molecules may be incorporated.<sup>8</sup> These guests alone are often antimicrobial, and are regularly comprised of metal ions or oxides, e.g. silver ( $\text{Ag}^{2+}$ ), zinc ( $\text{Zn}^{2+}$ ), zinc oxide ( $\text{ZnO}$ ), copper ( $\text{Cu}^+$  or  $\text{Cu}^{2+}$ ) or nickel ( $\text{Ni}^{2+}$ ). The MOF structure may biodegrade, and antimicrobial components may be gradually released via a constant mechanism. If this occurs with a sustained effect, and if both the ligand and guest molecules are antimicrobial, a combination of biocidal properties may result in synergistic effects. The combination of antibacterial substances and gases, e.g. nitric oxide ( $\text{NO}$ ), demonstrates this. Within mammalian biology,  $\text{NO}$  plays a key biological role as a signaling molecule though is also known to be toxic in excess amounts. When released from a MOF, localised (as opposed to systemic) effects occur. Using MOFs such as M-CPO-27, allows  $\text{NO}$ 's controlled release. Due to the behavior of the adsorption-storage-delivery cycle, unwanted side effects observed in previously trialed methods can be avoided. These methods used zeolites and functionalised silica nanoparticles as  $\text{NO}$  delivery vehicles, though led to the production of carcinogenic and pro-inflammatory side-products.<sup>7, 125-127</sup> MOFs are also favoured over metal-ion loaded natural and synthetic polymers due to their uniformity of speciation and their distribution of metal active sites. Furthermore, the strong stability of MOFs in the presence of oxygen and water inspires their potential for use in antimicrobial dermatology. MOFs could be applied as excipients in the preparation of topical bactericidal formulations or may act as active ingredients, which improve their adhesion and penetration.<sup>8</sup> Their controlled and prolonged molecule release could then improve that of poorly absorbing substances, which otherwise require multiple applications to achieve and maintain a sufficient activity level.

When considering the immobilisation of MOFs on different materials, e.g. silicones or textiles, new promising antimicrobial products may be developed. Novel investigations have described the antimicrobial potential of post-synthetically

modified ZIF-8.<sup>9, 128</sup> Redfern et al. in particular, outlined the potential of ZnO@ZIF-8 against common CAUTI-causing pathogens, finding that 0.8 mg mL<sup>-1</sup> ZnO was required to exhibit an antimicrobial effect, whilst ZIF-8 exhibited no bactericidal ability alone. When combined to form ZnO@ZIF-8, an MBC of 0.25 mg mL<sup>-1</sup> was obtained and the MOF demonstrated the ability to reduce the number of living cells in each bacterial biofilm tested to below the limit of detection (BLD, a 6 to 8 log decrease compared to exposure to control solution), over a 24 hour period, at the highest tested concentration of 2 mg mL<sup>-1</sup>. When incorporated into silicone elastomers, varied levels of antimicrobial action were observed across a range of CAUTI-causing pathogens. It was stated that if ZnO@ZIF-8 is able to prevent or delay bacterial growth on silicone material, the effect on consequent CAUTIs could be significant.<sup>9</sup> Nigar and Deniz however, investigated the bactericidal effects of polyurethane/ZIF-8 (PU-ZIF-8) coated fabrics against *Staphylococcus aureus*, concluding that PU-ZIF-8 nanocomposite-coated polyester fabrics had both antibacterial abilities and mechanical stability.<sup>9, 128</sup> Development of antibacterial wound dressings and medical devices could help benefit the medical industry significantly.<sup>9, 129</sup> In these cases, the antimicrobial material should also prevent the adhesion of bacteria to surfaces, thus preventing biofilm formation.

Post-synthetic modification of MOFs may enhance any biocidal capabilities of the original structures alone.<sup>130-132</sup> In the case of ZnO@ZIF-8, ZnO is already broadly accepted to house antimicrobial abilities. Combining this with ZIF-8 at a nanoparticle size, houses the potential for developing a notable biocidal material. Recent work investigated this and also provided evidence of non-toxicity. The antimicrobial potential of the precursor ZIF-8, or any potential mechanisms of action, however, were not discussed.<sup>9</sup> Despite this, Yamamoto and Zhang et al. have both suggested antimicrobial mechanisms for ZnO nanoparticles.<sup>133, 134</sup> Yamamoto, used *Staphylococcus aureus* and *Escherichia coli* to examine the antibacterial properties of various-sized ZnO nanoparticles. It was stated that antibacterial activity increased as the ZnO particle size decreased, since hydrogen peroxide, H<sub>2</sub>O<sub>2</sub>, was generated from water on the ZnO surface active centers. Facile penetration of H<sub>2</sub>O<sub>2</sub>, through the bacterial cell walls, caused damage to their structure and resulted in cell lysis.<sup>133</sup> In the case of urinary catheterisation, it may be possible for the same mechanism to occur within the catheter tubing. Furthermore, as bacteria are destroyed, the outward flush of patient urine may help prevent or reduce biofilm formation. Zhang

et al. reported a similar trend, though established that the concentration of ZnO particles was the primary factor responsible for biocidal activity, rather than the particle size of ZnO.<sup>134</sup>

Investigations into ZIFs with antimicrobial effects have also suggested alternative biocidal mechanisms. With regards to post-synthetically modified ZIF-8, the ZIF structure reportedly collapses to provide a sustained antibacterial effect and high durability.<sup>56</sup> Zn<sup>2+</sup> ions are gradually released, and metal agglomeration and oxidation are prevented. This is seen in the case of ciprofloxacin (CIP) -loaded ZIF-8 (CIP-ZIF-8). Here, antibacterial action results from the gradual degradation of the ZIF-8 structure, and the release of Zn<sup>2+</sup> ions and CIP, resulting in the physical destruction of the bacterial cell wall.<sup>8, 56</sup> Since a combination of the mechanisms outlined above, may apply to ZnO@ZIF-8, it is plausible that modified MOFs and ZIFs house extraordinary antimicrobial advantages over metal/metal oxide NPs alone. Such materials would find a wide range of clinical applications and recently, a patent has been granted involving the development of antimicrobial coatings formed from ZIFs.<sup>135</sup>

## **1.6. Silicone Polymers for Medical Use**

Synthetic polymers with basic repeating units of "siloxane" are generally categorised as silicones.<sup>136</sup> "Siloxane," refers to units of silicon to oxygen bonds, with silicon atoms bonded to organic groups. The most common of these is polydimethylsiloxane (PDMS), whose structure sees two methyl groups bonded to each silicon.<sup>137</sup> Due to the combination of an inorganic backbone and organic branches, silicones house unique properties, e.g. chemical and thermal stability, hydrophobicity and low surface tension, making them particularly durable and biocompatible.<sup>138</sup> As such, silicones may be used as compounds, fluids, emulsions, resins, and elastomers with abounding applications across diverse fields, having been commercially available for use in medical applications since 1946.<sup>136, 139</sup>

Elastomers of silicone are amorphous, viscoelastic polymers, formed by means of a cross-linking reaction, allowing the formation of chemical bonds between adjacent chains. This results in a three-dimensional network, usually achieved by one of three main methods: cross-linking with radicals, cross-linking by condensation or by cross-linking by addition.<sup>136</sup> Composites in this project were formed using a platinum (Pt) catalyst. This resulted in cross-linking by addition in order to exhibit properties such

as flexibility and durability, suitable for use in urinary catheterisation. Generally, elastomers contain extremely weak inter-molecular forces and have a low Young's modulus, alongside a high failure strain, in comparison to other materials.<sup>139</sup> In this work, cross-linking was achieved by reacting vinyl end-blocked polymers with Si-H groups carried by a functional oligomer (**Fig. 3**). Addition mostly occurs on the terminal carbon and is catalysed by the Pt metal complex. No by-products result.

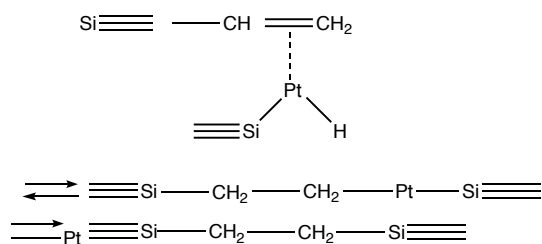


**Figure 3: Mechanism showing the oxidative addition of the  $\equiv\text{Si}$  to the Pt, H transfer to the double bond, and reductive elimination of the product. To simplify, other Pt ligands and other Si substituents have been omitted. Image adapted from Colas and Curtis, 2004.<sup>136</sup>**

This method produces accurately moulded pieces of silicone without shrinkage, however caution is required as the Pt catalyst may bond readily to electron-donating substances (such as amines), to form stable complexes with these “poisons”. This would render the catalyst inactive and inhibit the cure. Platinum cure cross-linking by addition is commonly used for the development of precise silicone parts.<sup>136</sup>

Furthermore, most silicone elastomers incorporate “filler”. This acts as both a material extender and reinforcement to the cross-linked matrix. Without it, the resulting silicone polymer would be weak and often unsatisfactory for most applications.<sup>140</sup> For elastomers with medical applications, fumed silica remains the filler of choice, and reinforcement results from polymer adsorption by the silica's large surface area. Hydroxyl groups on the filler's surface form hydrogen bonds between the filler and the silicone polymer, thus leading to elastomers with high tensile strengths and elongation capabilities.<sup>136</sup>

By adding reinforcing fillers, silicone's stickiness is reduced, hardness is increased, and mechanical strength is enhanced. The tiny spheroid silica particles ( $\sim 10$  nm diameter) fuse irreversibly whilst semi-molten, and form aggregates.<sup>136</sup> These become physically entangled on cooling and cure as agglomerates. The

incorporation of silica filler into silicone polymers increases the polymer's already high viscosity and is widely known as "compounding".

Previous studies successfully incorporated 2 wt.% and 4 wt.% ZnO@ZIF-8 within maxillofacial silicone, M511 (Technovent, UK), and demonstrated varied antimicrobial efficacy against common CAUTI-associated pathogens.<sup>9</sup> The mechanical properties of these composite silicone elastomers were not investigated.

### **1.7. Aims and Objectives**

The aim of this study was to incorporate antimicrobial porous materials, in the form of ZIF-8s, into silicone composite samples, then determine their ability to kill a CAUTIs- relevant pathogen, *E. coli*.

ZIF-8 structures of different particle sizes were to be prepared by both organic and aqueous syntheses, prior to modification and investigation into their antibacterial ability. These materials would be characterised by techniques such as X-Ray diffraction (XRD), Scanning Electron Microscopy (SEM) and Brunauer-Emmett-Teller (BET) surface area measurements, in order to qualitatively determine their size, structure and characteristics.

Selected ZIF-8 samples would then be post-synthetically modified by AgNO<sub>3</sub> treatment for further studies. This resulted in the preparation of ZnO@ZIF-8, which also required characterisation. Samples of each precursor ZIF-8 were kept for comparison.

Antibacterial activity of ZIF-8 and ZnO@ZIF-8 structures would be screened by means of minimum bactericidal concentration assays. Selected ZIF samples were then incorporated into composite silicone elastomers containing 4 wt.% of biocide. The antibacterial activity of ZIF-8- and ZnO@ZIF-8-loaded silicones would then be assessed, using BS ISO 22196:2011, to determine their potential use as biocidal additives to polymers. Their conformability, in terms of mechanical properties, would be evaluated.

Inductively Coupled Plasma Mass Spectrometry (ICP-MS), would then qualitatively determine any Zn-release concentrations of both powdered and embedded ZIF samples, following a prolonged period of incubation. The remaining powdered samples would then be re-characterised by XRD.

## CHAPTER 2: EXPERIMENTAL

### 2.1. Synthesis of ZIF-8 and ZnO@ZIF-8

Synthesis of ZIF-8 and ZnO@ZIF-8 was achieved through both organic and aqueous routes.

Organic synthesis for ZIF-8 was achieved through an adaptation of methods reported by Cravillon et al, whom stated an approximate molar ratio of 1:8:700 when  $\text{Zn}(\text{NO}_3)_2\text{:Hmim:MeOH}$  was used.<sup>90</sup>

Typically, 2.933 g of  $\text{Zn}(\text{NO}_3)_2\cdot 6\text{H}_2\text{O}$  and 6.4893 g of 2-methylimidazole (Hmim) were each dissolved in 150 cm<sup>3</sup> of the organic solvent chosen (methanol (MeOH), industrial methylated spirit (IMS) or N,N-Dimethylformamide (DMF)). The latter clear solution was then poured into the former clear solution, under vigorous stirring using a magnetic bar. Spontaneous formation of a milky solution was observed on mixing and stirring was ceased after 1 hour. The resulting solid was then separated from the by centrifugation at 6000 rpm for 10 minutes and washed thrice using fresh MeOH and centrifugation each time. To ensure sufficient washing, the product was ultrasonicated until complete redispersion was observed, prior to centrifugation. The product was dried overnight in an oven at 80°C.

In another method, ZIF-8 was prepared using an aqueous system, which required various volumes of triethylamine (TEA). This method was modified from Nordin et al.<sup>87</sup>, whereby a molar ratio of 1:6:500 of  $\text{Zn}(\text{NO}_3)_2\text{:Hmim:H}_2\text{O}$  was used.

Typically, 2.00 g (6.72 mmol) of  $\text{Zn}(\text{NO}_3)_2\cdot 6\text{H}_2\text{O}$ , was dissolved in 20 wt.% total deionised water (12.11 g), whilst simultaneously, 3.312 g (40.43 mmol) of Hmim, was dissolved in the 48.45 g deionised water remaining. The following volumes of TEA were then added to the Hmim solution, each in separate reactions: 1 cm<sup>3</sup>, 2 cm<sup>3</sup>, 3 cm<sup>3</sup>, 4 cm<sup>3</sup>.

Both solutions were then stirred vigorously for 30 minutes at room temperature. The product was then collected by centrifugation at 3000 rpm for 30 minutes, then washed repeatedly with deionised water, ultrasonication and centrifugation until a neutral pH was shown. Universal indicator paper was used. The remaining solid was then dried overnight in an oven at 60°C.

All samples were characterised (as detailed below in 2.2.), in order to confirm product purity before proceeding to form ZnO@ZIF-8 structures.

Once confirmed pure, ZnO@ZIF-8 was formed from the ZIF-8 by the following means, regardless of the prior synthesis route:

A solution of silver nitrate, AgNO<sub>3</sub> (53.7 mmol) was made in Milli-Q ultrapure water: ethanol (v/v = 1:6).

1.00 g of ZIF-8 was then added to 35.00 cm<sup>3</sup> AgNO<sub>3</sub> solution, in a foil-covered beaker and stirred continuously for 12 hours. The resulting solid was then separated by centrifugation at 6000 rpm for 40 minutes and washed four times using absolute ethanol (200 mL total volume) and centrifugation, each time. To ensure sufficient washing, the product was ultrasonicated until complete redispersion was seen. The product was air-dried in a fume cupboard at room temperature and pressure.

#### 2.1.1. Upscaling synthesis

Throughout this project the syntheses of neither ZIF-8, nor ZnO@ZIF-8, were scaled-up systematically. Instead, multiple reactions following the synthesis routes and conditions detailed above were established in tandem, with the aim of producing a combined batch for each required sample. In total, 32 reactions were conducted for the organic (MeOH only) synthesis method, yielding a total of 20.17 g ZIF-8. 15 aqueous reactions, each using 3cm<sup>3</sup> TEA, were required to produce 25.89 g ZIF-8. In turn, 10 reactions for each form of ZnO@ZIF-8 (both synthesis route) were run, producing 6.02 g and 7.36 g of ZnO@ZIF-8, respectively.

#### 2.1.2. Calcining products

All MOF compounds used in further investigations were ground with a pestle and mortar, then subject to calcining by means of continuous heat (200°C), for five hours, in air. This was conducted in an oven, at a heating rate of 10°C/min. This aimed to evacuate guest-molecules from samples formed using TEA, which may have been trapped within each structure's pores. ZIF-8 formed using methanol is reportedly guest-free.<sup>90</sup>

## 2.2. Characterisation of Samples

All samples were ground finely, using a pestle and mortar, prior to characterisation. In preparation for analysis by Scanning electron Microscopy (SEM) and Energy-Dispersive X-Ray Spectroscopy (EDX) each sample was mounted upon a carbon tab.

Those samples for SEM only were sputter-coated with Au using a Polaron SC7640 SEM Coating System, 800 V for 30 seconds at 5 mA.

SEM was used to investigate the morphology and particle size of each sample's structure. Using a Supra 40VP (Carl Zeiss Ltd.) and the software, SmartSEM.

EDX was conducted on all ZnO@ZIF-8 samples using an Apollo 40SDD (EDAX Inc.), using the Genesis software. This measured elemental compositions of the metal oxide composites and potential Ag concentrations, which may have remained from previous amalgamation. For each element present, the mean percentage weight was derived from five random areas per sample.

X-Ray diffraction (XRD) patterns for each crystalline sample were obtained using a PANalytical X'Pert diffractometer fitted with a PixCEL 1-D detector using a Cu anode ( $\lambda = 1.5406 \text{ \AA}$ ) with the generator set at 40 mA, 40 kV. Flat powder samples were prepared and measured in reflection geometry in the range  $5\text{-}120^\circ 2\theta$  with a step size of  $0.013^\circ 2\theta$  and a collection time of 118 s/step using automatic divergence and anti-scatter slits with an observed length of 5.0 mm. Data was processed using HighScore Plus version 4.7 (PANalytical BV, Delft, Netherlands, 2017).

Nitrogen adsorption-desorption measurements were taken at  $-196^\circ\text{C}$ , using a Micromeritics ASAP 2020 surface area analyser. Samples were degassed at  $200^\circ\text{C}$  overnight, prior to analysis. Using the BET equation in the 0.05-0.3 range of relative pressures, and the BJH (desorption branch of the isotherm) method, specific surface areas and pore size distributions were calculated. Total pore volumes ( $V_{\text{total}}$ ) were obtained from the volume adsorbed at a relative pressure of 0.99, whereas micropore volumes ( $V_{\mu}$ ) and BET surface areas ( $S_{\text{BET}}$ ) were determined from t-plot analysis.

### **2.3. Antimicrobial Testing of ZIF-8 and ZnO@ZIF-8**

Antimicrobial tests of each selected sample were conducted as detailed below.

#### **2.3.1. Maintenance and standardization of microorganisms**

*Escherichia coli* (*E. coli*, NCTC 9001) was maintained on Luria-Bertani (LB) agar (BD, Sparks, MD), at  $4^\circ\text{C}$ .

For the 'minimum bactericidal concentration assay' (MBC), a single colony of *E. coli* was inoculated into 25 mL of Luria-Bertani (LB) broth and grown  $22\pm 1$  hours at  $37^\circ\text{C}$  with agitation (180 rpm). Cells were then harvested by centrifugation (3600 rpm,

10 minutes) and resuspended in LB broth to an optical density of 0.025 at 600 nm, using a Jenway 6305 Spectrophotometer, UK.

For the 'measurement of antibacterial activity on composite samples' assays, a single colony of *E. coli* was inoculated into 25 mL of Luria-Bertani (LB) broth and grown  $22 \pm 1$  hours at 37°C with agitation (180 rpm). Cells were then harvested by centrifugation (3600 rpm, 10 minutes) washed once in 0.85% NaCl (Oxoid, UK) and resuspended in 0.85% NaCl (Oxoid, UK) to an optical density of 0.025 at 600 nm.

For both assays, an average suspension concentration of  $2.8 \times 10^7$  CFU mL<sup>-1</sup> resulted.

### 2.3.2. MBC assay

The commonly used MBC assay determines the minimum amount of an antimicrobial compound that is sufficient to reduce bacterial survival in a planktonic (that is, bacteria floating as single cells in water) culture.<sup>141</sup> For the purpose of this investigation, the MBC obtained was considered to be the lowest concentration of a compound able to kill all cells present (i.e. zero cells were recovered on fresh agar). Suspensions of the following compounds, at concentrations of 4 mg mL<sup>-1</sup>, were repeated technically in triplicate, and then biologically repeated once, **Table 1**.

**Table 1: Sample key for materials tested by MBC assays.**

Sample Number	Material
1	ZIF-8 from MeOH synthesis
2	ZIF-8 from MeOH synthesis (Calcined)
3	ZnO@ZIF-8 derived from Sample 1
4	ZnO@ZIF-8 derived from Sample 2
5	ZnO@ZIF-8 derived from Sample 2 (Calcined)
6	ZIF-8 from TEA (3cm <sup>3</sup> ) synthesis
7	ZIF-8 from TEA (3cm <sup>3</sup> ) synthesis (Calcined)
8	ZnO@ZIF-8 derived from Sample 7
9	ZIF-L
10	ZnO@ZIF-L derived from Sample 9

Each sample was suspended in sterile distilled water to a concentration of 4 mg mL<sup>-1</sup>. A doubling dilution was performed to a concentration of 7.63x10<sup>-6</sup> mg mL<sup>-1</sup>, leaving a 100 µL volume of each dilution in its corresponding well. 100 µL of standardised *E. coli* in LB broth (as described above) was added to each well and each 96-well plate was covered with a lid. These were incubated static, at 37°C for 18 hours. As a negative control, 100 µL of culture plus 100 µL of sterile distilled water was used. Following incubation, 20 µL aliquots were taken from each well, pipetted onto quartered LB agar plates, and spread evenly prior to static incubation (37°C) for a further 24 hours. The MBC was recorded as the lowest concentration at which growth was prevented. In total, six technical repeats were conducted - three for each biological repeat.

#### **2.4. Synthesis of Composite Samples**

The best performing samples from MBC assay results were selected for incorporation into silicone composite samples, alongside their ZIF-8 or ZnO@ZIF-8 counterparts. Prior to use, each of these were dried in an oven at 100°C, overnight. Composite samples were prepared using M511 maxillofacial material (Technovent, UK). Composites contained a mixture of 29.33 g Part A (Silicone polymer with Si-H groups) and 3.66 g Part B (vinyl functionalised dimethyl silicone polymer, plus Pt catalyst). This resulted in a ratio of 8:1, Part A:Part B. It should be noted that all commercial silicone elastomers contain fumed silica reinforcement. The M511 contains a small amount of fumed silica reinforcing filler, without which, tensile strength would be almost uselessly low. When incorporating ZIF materials, 1.32 g (4 wt.%) was added and stirred under vacuum for 5 minutes using Multivac 4 (Degussa AG, Germany). The uncured composite was then allowed to settle under vacuum, prior to spreading into a 13 cm x 13 cm x 0.2 cm metal mould, positioned atop a polytetrafluoroethylene (PTFE)-coated sheet, using a pallet knife. This was then placed upon a vibrating table for 10 minutes. All air bubbles produced were burst using a scalpel and a second PTFE sheet was used to sandwich the mould. This was then cured for 1 hour at 100°C, under 10 Ton, using a Bradley and Turton hydraulic press. The sample was allowed to cool to room temperature and then eased out of the mould gently.

#### **2.5. Assessment of ZIF Particle Dispersion Quality**

The dispersion quality of ZIF-8 and ZnO@ZIF-8 particles was assessed at two size scales; macro-dispersion was assessed qualitatively using digital images, whilst the micro-dispersion quality was assessed using the SEM images of the freeze-fractured surfaces taken at 50,000 times magnification.

#### 2.5.1. Macro-dispersion

Digital images were obtained using a Samsung Galaxy S6 Edge mobile phone camera, clamped above a black tile for consistent height. 1.2 cm x 1.5 cm coupons of each composite sample were photographed against the black tile, alongside two perpendicular rules for scale. Macro-dispersion qualities of the ZIF-8 particles were observed from these images.

#### 2.5.2. Micro-dispersion from freeze-fracture analysis

The micro-dispersion of the ZIF-8 particles was assessed by SEM imaging of freeze-fractured surfaces, prepared as follows: A 1 cm x 1 cm x 0.1 cm coupon was cut from each composite sample, as well as from a control sample of cured, unfilled matrix. Each coupon was then frozen in liquid nitrogen and fractured into two pieces. The fractured coupon was then mounted to a tab and was sputter-coated, allowing the cross-sectional area of the fractured surface to be examined using SEM. Instrumentation and sputter-coating conditions remained as stated in Section 2.2.

### **2.6. Composite Properties**

#### 2.6.1. Percent mass hexane swelling and extractables

The matrix crosslink density is confounded with filler-matrix interactions - the fillers existing as both fumed silica and the incorporated ZIFs. Whilst these were known to affect the composites' hexane swelling behaviour, further investigation was considered worthwhile due to evidence that ZIFs affected curing characteristics of M511 (see Section 3.3.). This presented so significant, that an increase in crosslinker volume was necessary. Thus, it was anticipated that some fractions of the matrix may not be crosslinked.

The amount of crosslinked polymer was determined using the hexane extractables content. Hexane was the chosen solvent due to its close match to the Hansen Solubility parameter of polydimethylsiloxane (14.9  $\delta_d$  and 15.1  $\delta_d$ , respectively).

Hexane (Fisher) swelling measurements were carried out on the composite samples under ambient conditions. Sample coupons, with dimensions of 1 cm x 1 cm x 0.1 cm were used. Each coupon was weighed both before and after immersion in hexane for 24 hours. Each vessel was covered throughout the immersion time, in order to prevent solvent evaporation. Excess hexane was removed from samples using filter paper before weighing. The degree of swelling was calculated using equation 1.0.

$$\text{Swelling degree (\%)} = \frac{\text{weight after} - \text{weight before}}{\text{weight before}} \times 100 \quad (1.0)$$

Each coupon was then dried overnight in an oven at 70°C, prior to re-weighing and determination of the hexane extractables content. The equation 2.0 was used.

$$\text{Extractables content} = \frac{\text{mass before} - \text{mass of dried sample}}{\text{mass before}} \times 100 \quad (2.0)$$

### 2.6.2. Tensile testing

Tensile tests (N=5) were conducted at room temperature using a Hounsfield H10KS tensometer running Qmat 5.52 software. The instrument was fitted with a 100 N load cell and laser extensometer. Crosshead speed was 500 mm/min. BS903 type 2 dumb-bell specimens with a width of 4.0±0.1 mm were cut from each ~1 mm thick composite sheet. Test piece thickness was measured using a dial gauge.

Average stress-strain curves were plotted using Microsoft Excel, for each material using the raw strain and force data for each sample. Values of stress were calculated via using equation 3.0.

$$\text{Stress (MPa)} = \frac{\text{Force (N)}}{\text{Area (mm}^2\text{)}} \quad (3.0)$$

Values of tensile strain were provided by the QMAT 5.52 software and were present in the obtained raw data. Estimated values of Young's modulus were determined using linear regression from the initial linear region of the stress-strain curves. The linear region varied from between 0 to 10% and 0 to 30%. The Young's moduli

were determined for all five replicates, with the average and standard deviations deduced. Values of average tensile strength and elongation at break were also determined from the computer software generated values.

## **2.7. Antimicrobial Testing of Composite Samples**

### 2.7.1. Measurement of antibacterial activity on composite samples

The antibacterial activity of each composite sample was tested following an adapted protocol of the BS ISO 22196:2011. This protocol is the current international standard for evaluating the biocidal activity of antibacterial-treated plastics and other non-porous surfaces of products, such as the M511 maxillofacial silicone used in this study. Time points for sampling were conducted at 0, 3, 8 and 24 hours. For each composite, three 1 cm x 1 cm x 0.1 cm coupons were prepared per time point. These were cut to size using a scalpel and rule and sterilised using absolute ethanol. Each of these were then inoculated with 10  $\mu\text{L}$  of washed and standardized cell suspension (comprised from LB Broth), then covered gently with a 1 cm x 1 cm piece of polyethylene (PE) (SLS, Nottingham). Triplicates of covered coupons were carefully positioned in petri dishes then incubated at 37°C within a lidded container, lined with moistened paper towels, to create conditions of >90% humidity. At the appropriate time points, each sample coupon and its attached PE sheet was immersed in 10 mL neutralising buffer (15 g Tween80 [Sigma-Aldrich, Dorset] and 30 g Soya Lecithin [Optima Healthcare Lecithin, Holland and Barratt, UK.] dissolved in 1 L distilled water),<sup>142</sup> then vortex-mixed for 30 seconds. This ensured the removal of both the PE sheet, and most of the cells from the composite and PE surfaces, into the liquid. Use of the neutralising buffer prevented any further bactericidal action from the appropriate time point. The resulting bacterial suspension was diluted 10-fold (1 mL into 9 mL of sterile physiological saline), seven times, to a concentration of  $10^{-7}$  of the original suspension. 20  $\mu\text{L}$  of each dilution was then pipetted, in duplicate, onto quartered LB agar plates and spread evenly across the allocated agar surface using a loop. Plates were incubated for 18 hours at 37°C. The CFU  $\text{mL}^{-1}$  was then calculated following resultant colony counts. All samples were duplicated, and the experiment was repeated.

## 2.8. Metal Release Testing in Artificial Urine

For each composite material (including the control), a 1 cm x 1 cm x 0.1 cm coupon was submerged in 10 cm<sup>3</sup> artificial urine and sealed within a sterile universal container. This was incubated at 37°C, remaining stationary for 85 days. The coupon was removed by filtration, then Inductively Coupled Plasma Mass Spectrometry (ICP-MS) analysis was conducted on the filtrate remaining.

ICP-MS was conducted as follows, using an iCAP6300 DUO (Thermo Scientific), with the software package, Qtegra. A solution of artificial urine was prepared using the following: 0.20 g KCl, 8.00 g NaCl, 1.14 g Na<sub>2</sub>HPO<sub>4</sub> and 0.20 g KH<sub>2</sub>PO<sub>4</sub>. Deionised H<sub>2</sub>O was then added to form a total volume of 1.00 Litre. The pH of the solution was adjusted using HCl and NaOH, resulting in a final pH of 7.75.<sup>143</sup>

For each composite sample, corresponding crystalline powder samples were also tested. Solutions of each ZIF-8 and ZnO@ZIF-8 (4 mg/mL), were made using 10 cm<sup>3</sup> artificial urine and sealed within sterile universal containers. Likewise, these were incubated stationary for 85 days at 37°C. The sediment was then removed by filtration and ICP analysis of the filtrate was conducted as above. For further analysis, each crystalline sediment was recovered and air-dried prior to XRD investigation.

## CHAPTER 3: RESULTS AND DISCUSSION

### 3.1. Synthesis of ZIF-8

#### 3.1.1. Synthesis in organic medium

ZIF-8 samples were prepared in the presence of three different organic solvents; methanol, industrial methylated spirit and N, N-dimethylformamide, following synthesis routes adapted from Cravillon et al.<sup>90</sup> This enabled investigation into how the variation of organic solvent affected the purity, crystallinity and morphology of ZIF-8.

In contrast to other syntheses routes of nanoscale carboxylate-based MOFs, this simple organic method did not require any activation or auxiliary stabilising by means of heating or microwave/ ultrasound irradiation.<sup>144-146</sup> Instead, a room temperature synthesis was conducted, which required the addition of excess Hmim to the zinc source,  $Zn(NO_3)_2 \cdot 6H_2O$ , in each organic solvent. When using methanol, nanocrystals rather than larger microcrystals were formed, similarly detailed by Huang et al. and Park et al. in previous studies.<sup>60, 147</sup> XRD and SEM analysis was conducted on the resultant samples. Corresponding XRD patterns are illustrated in **Fig. 4** and SEM images are depicted in **Fig. 5**.

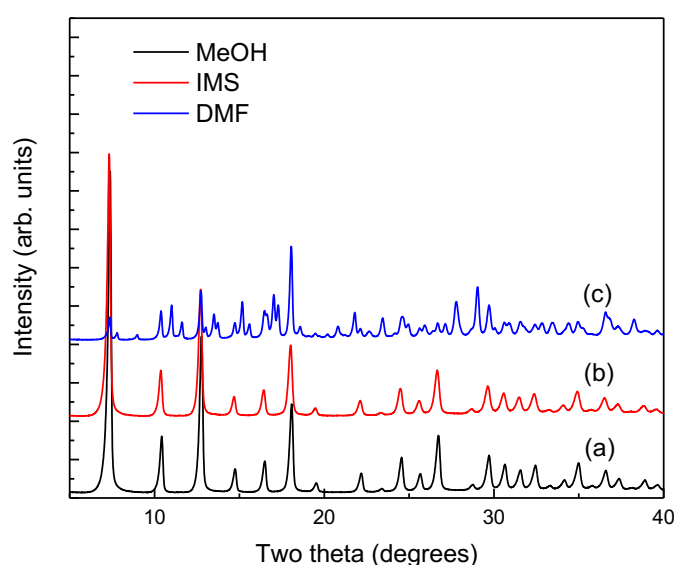


**Figure 4: XRD patterns of ZIF-8 samples prepared using (a) methanol (MeOH), (b) industrial methylated spirit (IMS) and (c) N, N-Dimethylformamide (DMF).**

Comparing these patterns to those reported by Cravillon et al. confirmed that synthesis routes using MeOH and IMS both resulted in the formation of pure, single-phase ZIF-8.<sup>90</sup> XRD patterns of the DMF synthesized sample however, highlighted the presence of impurities alongside smaller peaks at positions expected of pure ZIF-8.

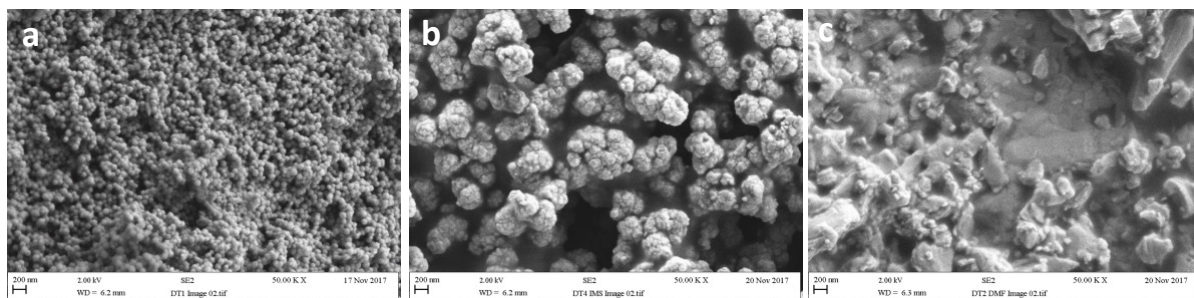


**Figure 5: SEM images of ZIF-8 samples prepared with: (a) MeOH, (b) IMS and (c) DMF solvents.**

The SEM images clearly showed round, uniform crystals of ZIF-8 from MeOH-based synthesis (**Fig. 5a**) each of  $\sim 60$  nm in size. These were slightly larger than those reported by Cravillon et al. measuring  $\sim 40$  nm, however similar rhombic dodecahedron ZIF-8 nanocrystals were obtained.<sup>90</sup> In contrast, **Fig. 5b** displayed slightly larger, irregular particles following synthesis using IMS. Peak widths in the XRD patterns remain closely similar between syntheses with MeOH and IMS, and the SEM images suggest crystallite sizes akin to one another. However, aggregates are clearly presented by the SEM image, in the case of the IMS solvent. Furthermore, **Fig. 5c** clearly showed the presence of other unknown crystal structures following reactions using DMF. Impurities highlighted by the XRD patterns above, were accredited to these irregular structures. For these reasons, only samples produced using MeOH as the organic solvent were carried forward for post-synthesis modification and further studies.

### 3.1.2. Synthesis in aqueous medium

ZIF-8 was also prepared in aqueous medium to reduce the use of large amounts of organic solvents as well as the amount of Hmim. Triethylamine (TEA), was added to the synthesis solution to facilitate the ZIF-8 formation. In accordance with previous results, adjusting the ratio of TEA within the reaction mixture effected the

size of ZIF-8 particles produced.<sup>87</sup> XRD patterns of samples prepared with varied amounts of TEA are shown in **Fig. 6**.

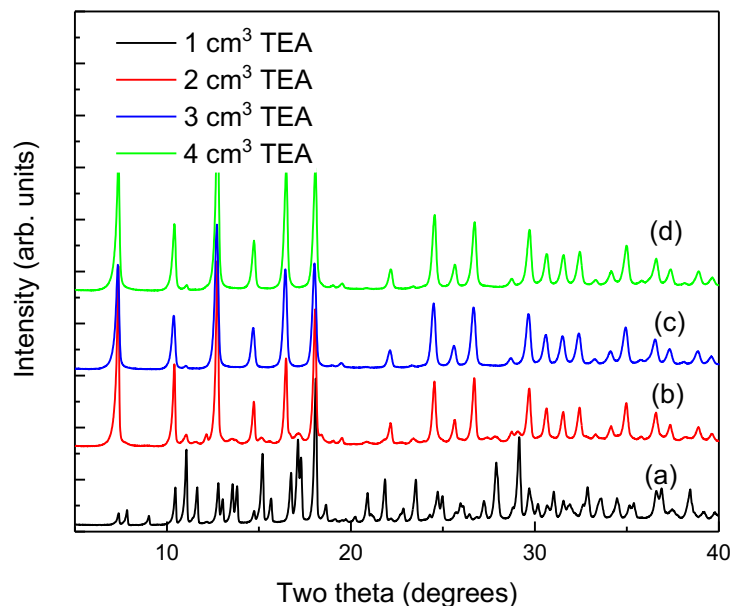


**Figure 6: XRD patterns of ZIF-8 samples prepared using 1 cm<sup>3</sup> - 4 cm<sup>3</sup> TEA (a-d, respectively).**

Comparisons of these peaks with those previously reported, confirmed the presence of pure ZIF-8 in samples made with 3 cm<sup>3</sup> and 4 cm<sup>3</sup> TEA.<sup>90</sup> Samples formed using 2 cm<sup>3</sup> TEA showed that formation of ZIF-8 was successful, though additional peaks suggested the presence of impurities. A reduction of TEA to 1 cm<sup>3</sup> however, presented XRD patterns which were absent of ZIF-8's characteristic peaks. This was supported by the literature, which purported three reasons for low TEA/total molar ratio (0 to 0.002) restricting the synthesis of ZIF-8.<sup>87</sup> Firstly, a low ligand to metal-salt ratio may result in intergrowth hinderance.<sup>148</sup> Secondly, insufficient ratios of Hmim in the solution may have impeded crystal growth and reduced the reaction rate, and finally; such low TEA/total molar ratio was insufficient to deprotonate the Hmim, producing more reactive sites on the ligands. Reactions with Zn<sup>2+</sup> were therefore obstructed.<sup>87</sup> Due to differences in the patterns achieved showing pure ZIF-8 and those obtained from synthesis with 1 cm<sup>3</sup> and 2 cm<sup>3</sup> TEA, these particular synthesis methods were disregarded from further study.

SEM analysis revealed a decrease in crystal size as the amount of TEA used increased. This is detailed in **Fig. 7** and confirmed in previous reports.<sup>87</sup> These further informed the preferred TEA volume (cm<sup>3</sup>) required for ZIF-8 formation.

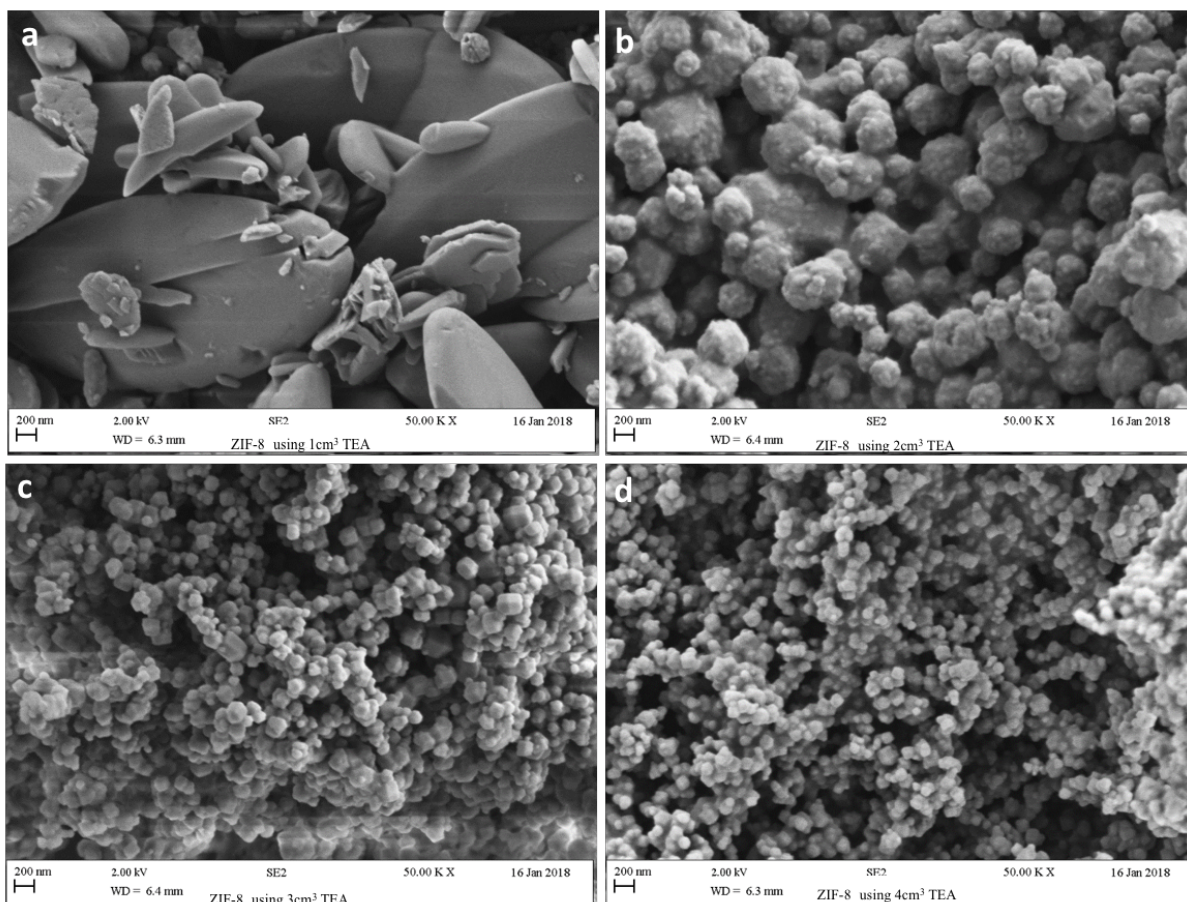


**Figure 7: SEM images from aqueous ZIF-8 synthesis using (a) 1 cm<sup>3</sup> TEA, (b) 2 cm<sup>3</sup> TEA, (c) 3 cm<sup>3</sup> TEA and (d) 4 cm<sup>3</sup> TEA. Scale bars indicate 200 nm.**

As depicted above (**Fig. 6** and **Fig. 7a**), aqueous synthesis using only 1 cm<sup>3</sup> TEA did not result in the formation of ZIF-8. Instead, mixed-phase crystals were shown - some 2D, elongated and 'leaf-like' in shape. Comparisons with the literature confirmed that these were ZIF-L structures, as opposed to ZIF-8.<sup>59</sup> Since these were formed from the same precursor materials but resulted in such different crystal sizes and morphologies, ZIF-L samples were also carried forward for further studies.

Structures displayed in **Fig. 7b**, showed irregularities and structural defects, as supported by XRD patterns in **Fig. 6**. Due to this, samples produced using 2 cm<sup>3</sup> TEA were eliminated from future investigation. Furthermore, **Fig. 7c** indicated the presence of noticeably larger ZIF-8 crystals (up to 250 nm) compared to those in

**Fig. 5a.** Despite confirming both samples formed using 3 cm<sup>3</sup> and 4 cm<sup>3</sup> TEA as ZIF-8, more uniform crystals were shown by those made using 3 cm<sup>3</sup> TEA. The trend in particle size to TEA/total molar ratio, remained a consequence of greater amounts of TEA, which promoted more nuclei formation via the deprotonation of Hmim. Rapid reactions between Zn<sup>2+</sup> and Hmim<sup>-</sup> encouraged the formation of small particles.<sup>85</sup> Investigations by Nordin et al. surmised that the highly concentrated synthesis solution led to rapid crystal formation with irregularities arising from the addition of TEA.<sup>87</sup> TEA deprotonates the organic ligand during ZIF formation, and thus controls crystal growth and particle size.<sup>59, 87</sup>

Additional analysis of ZIF-8 samples prepared with different TEA volumes was conducted using nitrogen adsorption data. Corresponding BET surface areas were calculated and listed in **Table 2**.

**Table 2: BET surface areas of ZIF-8 from organic and aqueous synthesis routes.**

ZIF-8 Synthesis Route	Surface Area (m <sup>2</sup> /g)
Organic using MeOH	1110
Aqueous using 1 cm <sup>3</sup> TEA	58
Aqueous using 2 cm <sup>3</sup> TEA	437
Aqueous using 3 cm <sup>3</sup> TEA	492
Aqueous using 4 cm <sup>3</sup> TEA	478

Values in **Table 2** are significantly lower than those reported by routes of similar organic synthesis (obtaining >1000 m<sup>2</sup>/g).<sup>90</sup> Low surface areas for the aqueously synthesised ZIF-8 suggested occluded TEA molecules and/or unreacted Hmim within the microporous framework. By calcining these samples, such guest molecules were evacuated. The sample prepared with 3 cm<sup>3</sup> TEA showed the highest surface area, and this sample was heat-treated at 200°C to remove the occluded TEA molecules. The surface area of this sample following heat-treatment increased to 1084 m<sup>2</sup>/g confirming the successful opening of the ZIF-8 porous structure. In addition, XRD patterns of this sample before and after the heat treatment (**Fig. 8**) showed the preservation of the ZIF-8 structure after heat-treatment, and an increase in the intensities of the ZIF-8 XRD peaks, in accordance

with the surface area results.

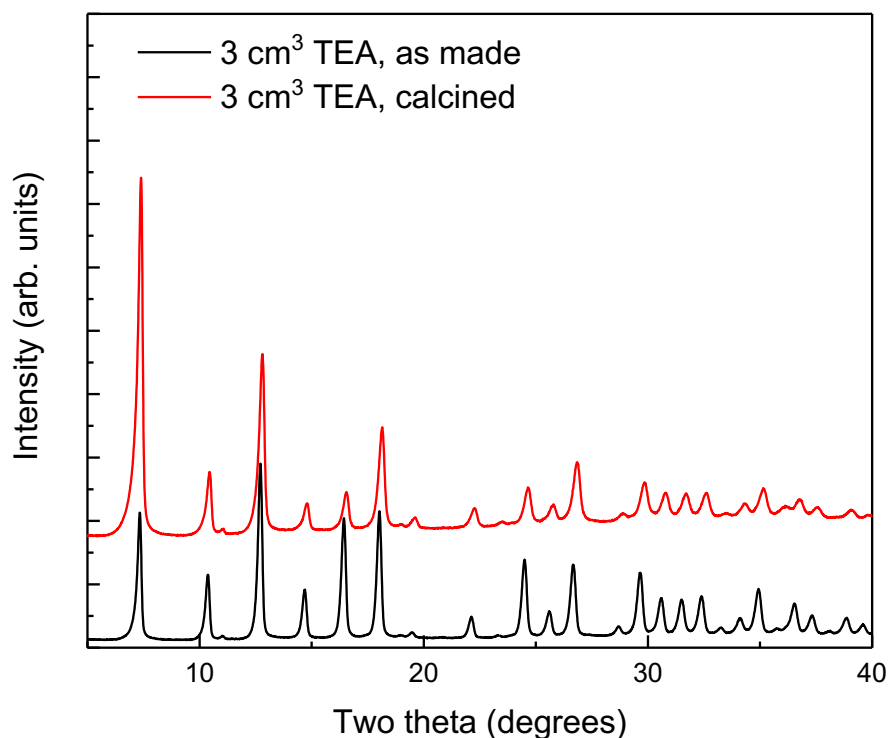


**Figure 8: XRD patterns of ZIF-8 prepared using 3 cm<sup>3</sup> TEA: (bottom) as-made and (top) heat-treated at 200°C.**

### 3.1.3. Post-synthetic modification of ZIF-8

The ZIF-8 prepared in MeOH (ZIF-8 (MeOH)), and in an aqueous medium in the presence of 3 cm<sup>3</sup> TEA (ZIF-8 (TEA)), were selected for post-synthesis modification with AgNO<sub>3</sub> to prepare ZnO@ZIF-8 structures. To minimise variations in the properties of the samples during microbiology experiments, samples were prepared in small batches and mixed together to obtain a large homogeneous batch of each sample. These were used in all further studies. Considerably more reactions in MeOH were required to obtain similar amounts of ZIF-8 as achieved from aqueous methods, since yields were reported to be 50% and 90%, respectively.<sup>87, 90</sup> Following this, samples of ZIF-8 from both routes were post-synthetically modified to obtain ZnO@ZIF-8. These were characterised and further tested alongside ZIF-8 in minimum bactericidal concentration (MBC) assays.

Half of the ZIF-8 (MeOH) and ZIF-8 (TEA) batches prepared were post-synthetically treated with silver nitrate solution to obtain ZnO@ZIF-8 (MeOH) and ZnO@ZIF-8 (TEA) samples as described in previous studies.<sup>9, 95</sup> The treatment resulted in the

spontaneous formation of ZnO nanorods within the ZIF-8 material. **Figs 9 and 10** show XRD patterns of ZIF-8 and ZnO@ZIF-8 batches, synthesised with MeOH and TEA, respectively.

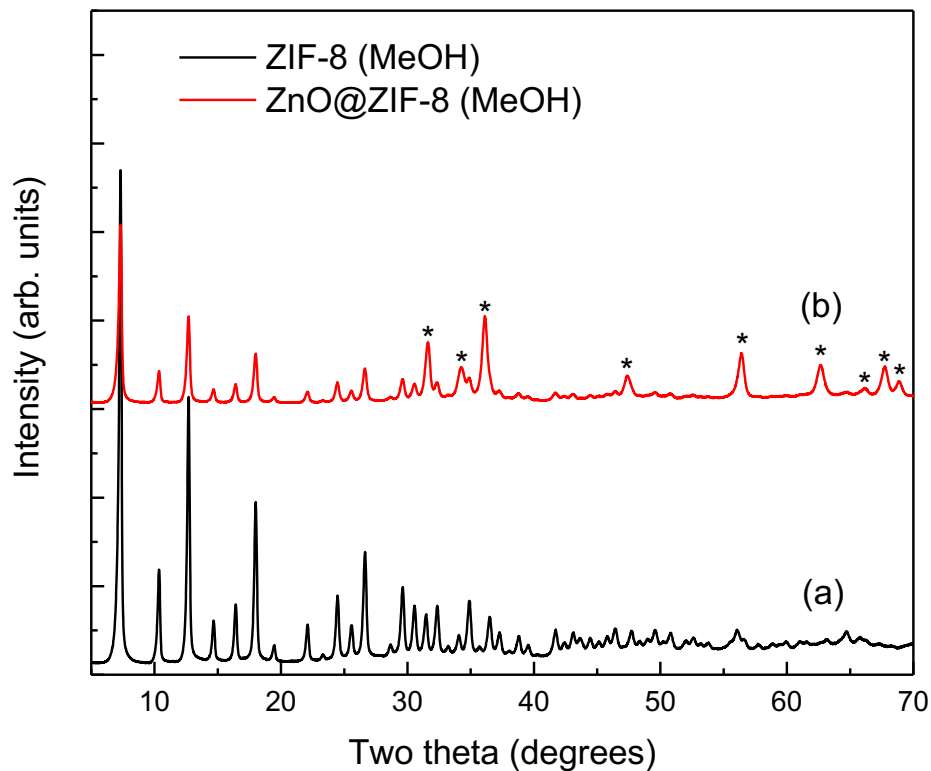


**Figure 9: XRD patterns of (a) batch ZIF-8 sample prepared using methanol and (b) the corresponding ZnO@ZIF-8 sample. The asterisk indicates ZnO XRD peaks (reference pattern 96-900-4182).**

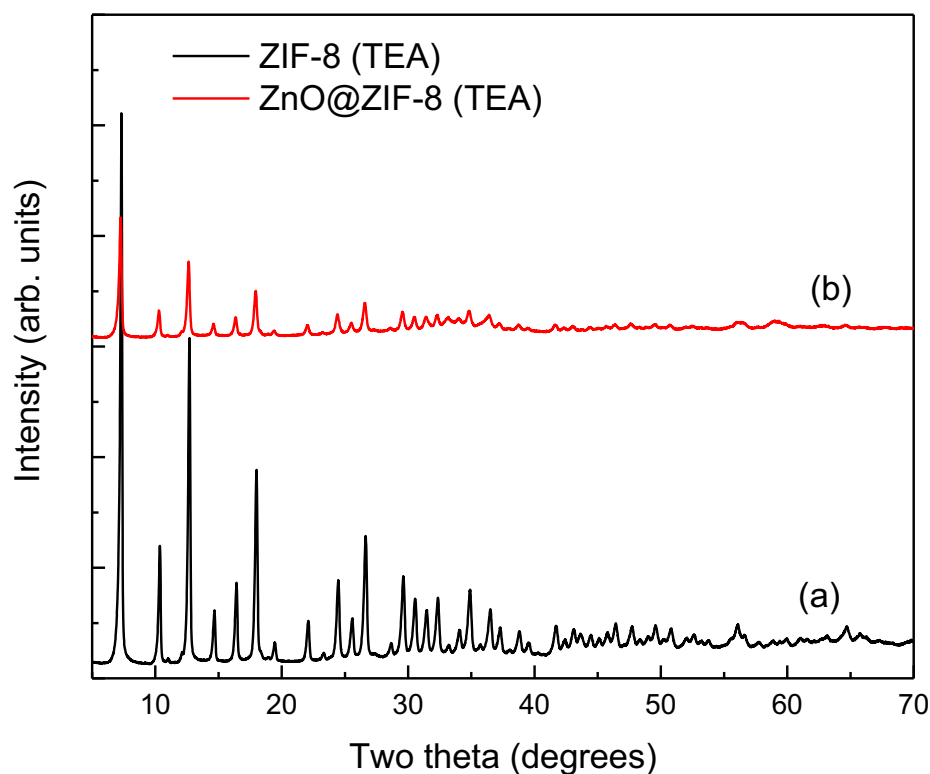


**Figure 10: XRD patterns of (a) batch ZIF-8 sample prepared from the 3 cm<sup>3</sup> TEA system and (b) the corresponding ZnO@ZIF-8 sample.**

In **Fig. 9**, peaks corresponding to the presence of ZnO were detected in accordance with previous results.<sup>9, 95</sup> The ZnO peaks were not detected in the ZnO@ZIF-8 sample prepared from ZIF-8 (TEA) (**Fig. 10**). Post-synthetic treatment of ZIF-8 reduced the intensity of the ZIF-8 peaks for both samples, which was more pronounced for the ZIF-8 (TEA) sample, indicating that silver nitrate treatment leads to an inferior level of crystallinity when compared to ZIF-8 alone. SEM analysis depicted in **Fig. 11** indicated the presence of ZnO nanorods in both ZnO@ZIF-8 samples (indicated by arrows in **Fig. 11a**). These ZnO nanorods are formed spontaneously during synthesis, upon the surface of the ZIF-8 crystals. The ZnO@ZIF-8 (MeOH) sample consisted of more rounded crystals compared to the rhombic dodecahedron ZIF-8 (MeOH) crystals in **Fig. 5**. ZnO-nanorods were clearly depicted in the SEM image of ZnO@ZIF-8 (TEA) sample (**Fig. 11b**) despite that they were not detected by XRD. In addition, impurities of amorphous material were also detected in this sample, which supported XRD patterns depicting inferior crystallinity of that sample.

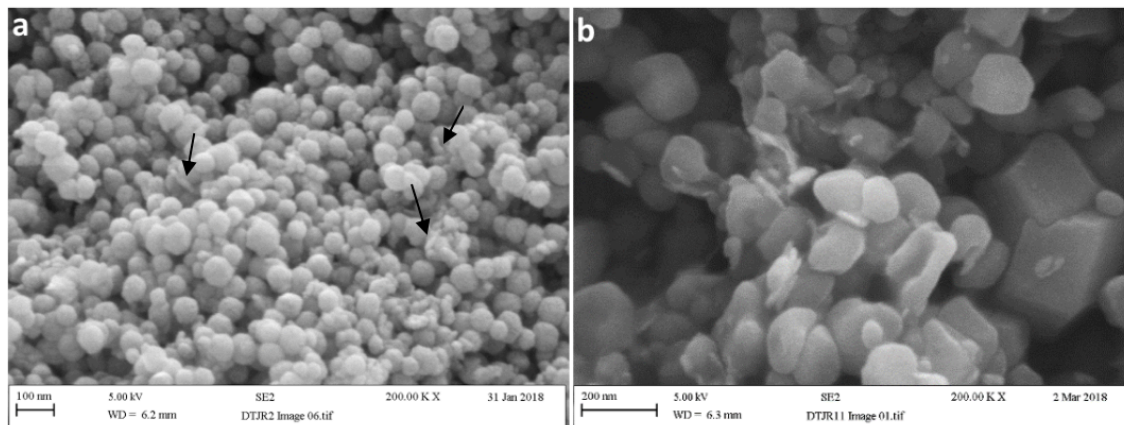


**Figure 11: SEM images of ZnO@ZIF-8 samples prepared with: (a) MeOH, (b) 3 cm<sup>3</sup> TEA.**

EDX analysis was used to determine whether Ag impurities were present in the post-modified ZIF-8 samples, which would influence their antibacterial activity and corresponding spectra are shown in **Figs. 12 and 13**. Peaks for C, N, O and Zn concur with the chemical composition of ZIF-8. Ag was not detected in the EDX spectrum of ZnO@ZIF-8 (MeOH) (**Fig. 11**). However, Ag was present in the ZnO@ZIF-8 (TEA) sample despite the repeated washing of this sample suggesting a stronger interaction between silver nitrate and ZIF-8 (TEA) (**Fig. 12**). These results also indicate that this post-synthesis treatment procedure does not give the same results for ZIF-8 materials prepared by different synthesis methods.

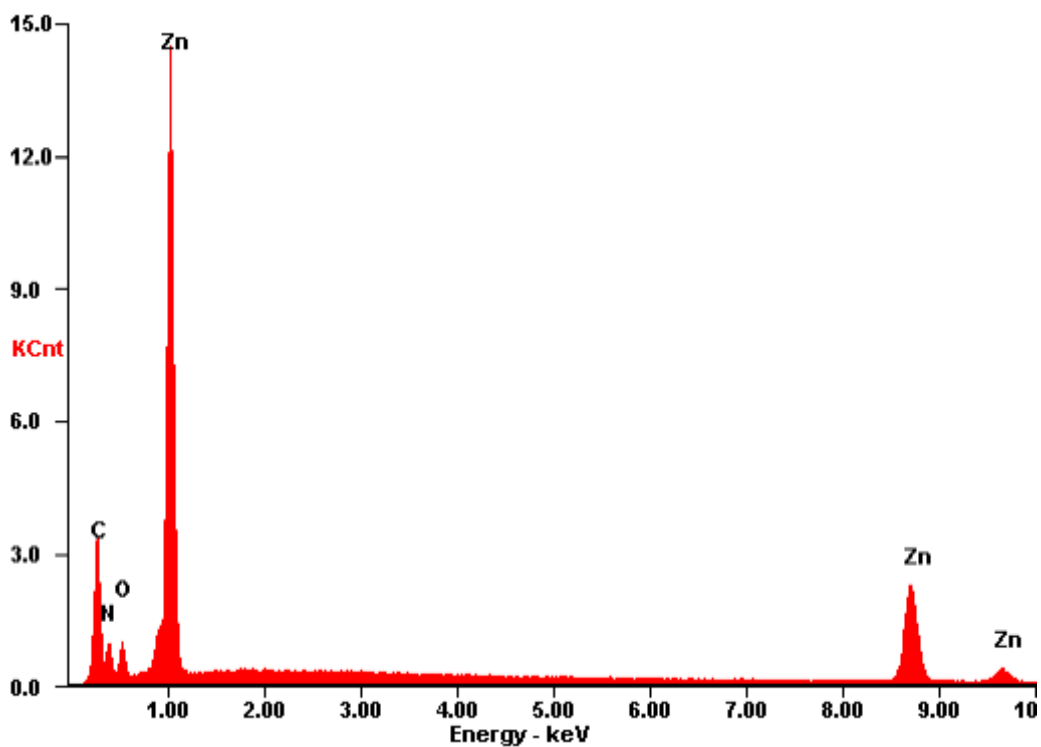


**Figure 12: EDX spectra of ZnO@ZIF-8 prepared using MeOH.**

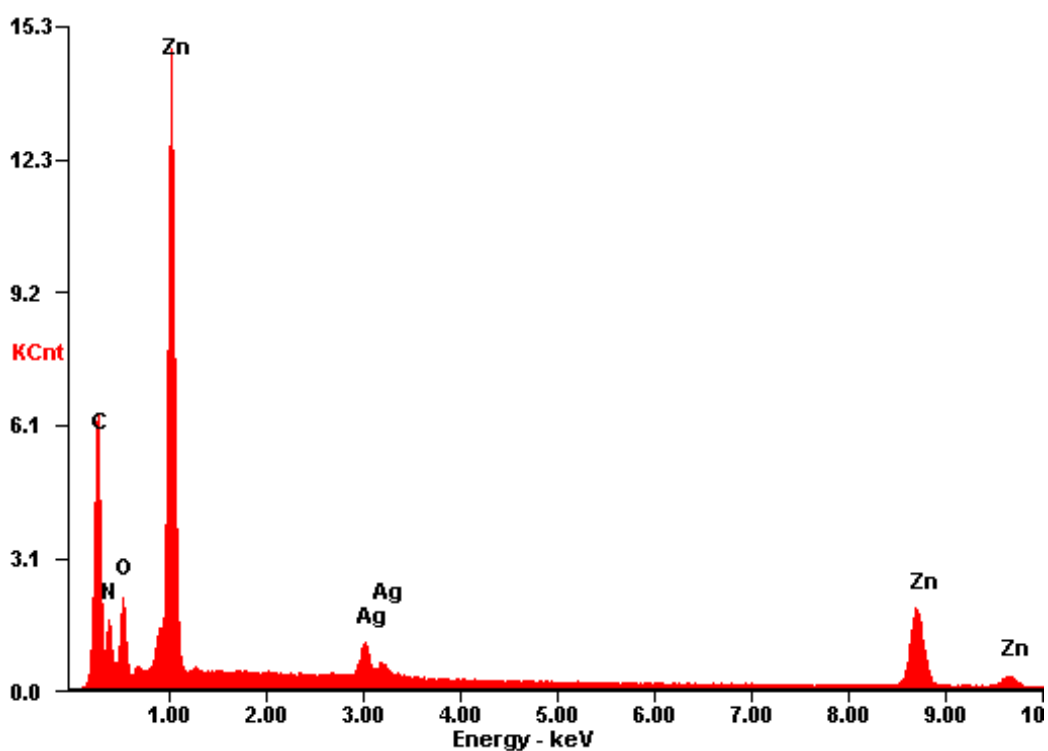


**Figure 13: EDX spectra of ZnO@ZIF-8 prepared using TEA.**

Analysis of batch-samples regarding BET surface areas ( $\text{m}^2/\text{g}$ ) and micropore volumes ( $\text{cm}^3/\text{g}$ ) is detailed in **Table 3**.

**Table 3: BET surface areas ( $S_{\text{BET}}$ ), total pore volumes ( $V_{\text{total}}$ ) and micropore volumes ( $V_{\text{micro}}$ ) of the four batch samples prepared.**

Sample and Synthesis Route	$S_{\text{BET}}$ ( $\text{m}^2 \text{g}^{-1}$ )	$V_{\text{total}}$ ( $\text{cm}^3 \text{g}^{-1}$ )	$V_{\mu}$ ( $\text{cm}^3 \text{g}^{-1}$ )
ZIF-8 prepared using MeOH	1293	0.99	0.58
ZnO@ZIF-8 prepared using MeOH	1000	1.02	0.42
ZIF-8 prepared using TEA	1280	0.81	0.59
ZnO@ZIF-8 prepared using TEA	769	0.82	0.32

ZIF-8 samples prepared by both methods were characterised by similar surface areas and micropore volumes in agreement with the XRD results. The silver nitrate treatment resulted in a decrease in the surface area and micropore volume, which was more pronounced for the sample prepared from ZIF-8 (TEA), again in agreement with the XRD results. The total pore volumes of each ZIF-8 framework increased marginally following silver nitrate treatment, which could be related to the formation of the ZnO nanorods. Nitrogen adsorption isotherms of the ZIF-8 samples before and after silver nitrate treatment are shown in **Figs. 15** and **16**. All isotherms were type I isotherms typical of microporous materials with a hysteresis loop at high relative pressures due to interparticle (textural) porosity. The decrease in the volume adsorbed at  $p/p_0 < 0.1$  for ZnO@ZIF-8 samples is related to the inferior crystallinity of the modified samples seen by the decreased intensity of the ZIF-8 peaks in the XRD patterns and also by the lower micropore volumes of these samples. This effect was more pronounced for the ZnO@ZIF-8 (TEA) sample. The hysteresis loop had a similar shape for ZIF-8 (MeOH) and ZnO@ZIF-8 (MeOH) samples (**Fig. 15**), indicating a similar interparticle porosity as seen by the SEM analysis (**Figs. 11a** and **5a**). The hysteresis loop for ZnO@ZIF-8 (TEA) is larger

compared to that of ZIF-8 (TEA) (**Fig. 16**), which can be associated with the different morphology of these two samples (**Figs. 11b** and **7c**).

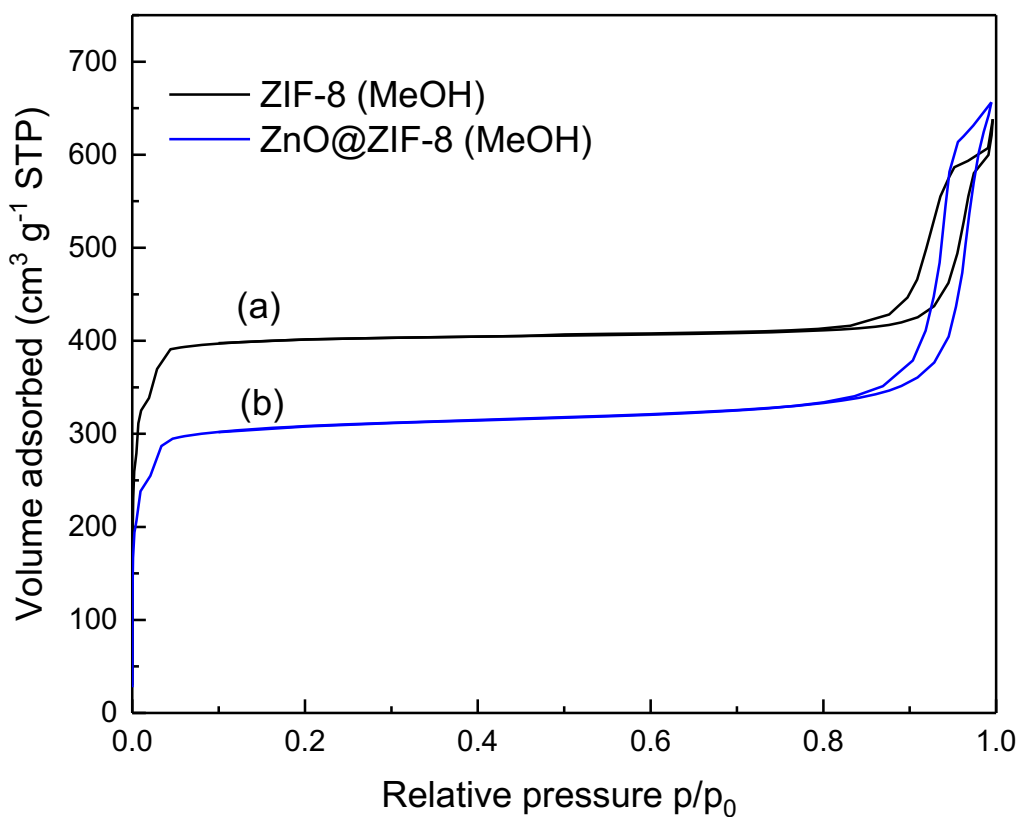


**Figure 14: Nitrogen adsorption-desorption isotherms at -196°C of (a) ZIF-8 (MeOH) and (b) ZnO@ZIF-8 (MeOH) samples.**

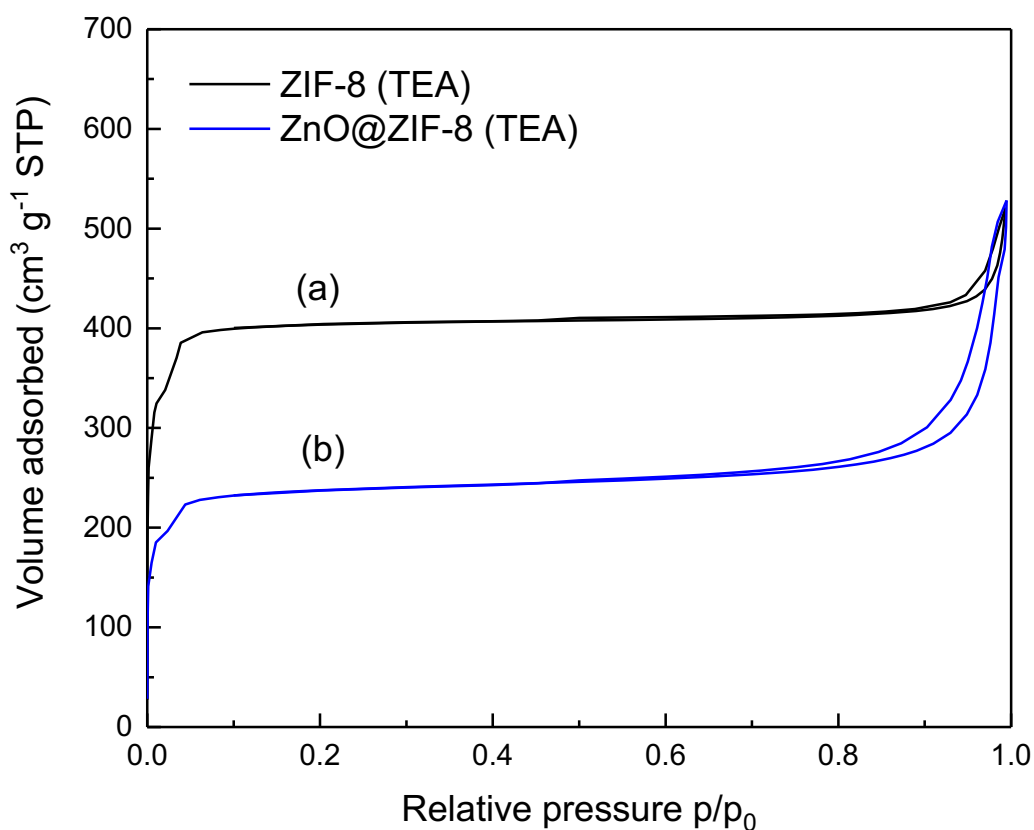


**Figure 15: Nitrogen adsorption-desorption isotherms at  $-196^{\circ}\text{C}$  of (a) ZIF-8 (TEA) and (b) ZnO@ZIF-8 (TEA) samples.**

In this study, ZnO@ZIF-8 samples adsorb significantly less  $\text{N}_2$  than the corresponding ZIF-8. This can be explained by the XRD and BET surface area data in **Figs 9 and 10**, and in **Table 3**, which shows a reduction in the ZnO@ZIF-8's surface area when compared to samples of ZIF-8. Greater structural collapse of the ZnO@ZIF-8 is also suggested by the isotherms, when compared to the parent ZIF-8.

Hysteresis loops are commonly attributed to the thermodynamic effects, network effects, or a combination of both. With each hysteresis shown above, agglomerates or spherical particles are suggested to be arranged in a fairly uniform manner with cylindrical pore geometries, thus indicating relatively high pore size uniformity. **Fig. 14 and Fig. 15** both display larger hysteresis loops for ZnO@ZIF-8 than for the parent ZIF-8. This is due to the presence of the ZnO-nanorods affecting the intraparticle (textural) porosity. These loops are associated with capillary condensation occurring within the mesopores and limiting uptake over a range of

high relative pressure ( $p/p_0$ ). At higher pressures, the slopes show an increased uptake of the adsorbate as the pores become filled.

### **3.2. Antimicrobial Testing of ZIF-8 and ZnO@ZIF-8**

#### 3.2.1. Minimum bactericidal concentration assay

MBC assays (**Table 4**) highlighted the differences in antibacterial potency of each selected framework. For ZIF-8, larger crystals with slightly lower BET surface areas displayed greater antibacterial activities. These structures were formed aqueously using TEA and presented more edge and corner sites than ZIF-8 synthesised organically. For ZnO@ZIF-8 samples, ZnO-nanorods are present (**Fig. 11**), which increase biocidal activity.<sup>9</sup> MBC assays of these structures corresponded to reports by Stanković et al., whom found that a higher concentration of smaller particles, with a larger surface area, ensures more efficient antibacterial behaviour when investigating properties of ZnO powders.<sup>149</sup> It is therefore likely that particle shape and crystalline structure have less influence on biocidal action than size and surface area.

**Table 4: Heat-mapped average MBC (mg mL<sup>-1</sup>) values of samples subjected to minimum bactericidal concentration assays, with sample numbers corresponding to Table 1. Green shows the lowest figures, with progression through amber to red as values increase.**

Sample Number	Sample Type	Average MBC (mg/mL)	Standard Deviation	Standard Error
1	ZIF-8	0.2340	1.4642	0.6548
2	ZIF-8	0.0709	0.2638	0.1319
3	ZnO@ZIF-8	0.0441	0.4634	0.2676
4	ZnO@ZIF-8	0.0228	0.0681	0.0393
5	ZnO@ZIF-8	0.0443	0.3210	0.1605
6	ZIF-8	0.0590	0.1649	0.1166
7	ZIF-8	0.0575	4.3524	1.7769
8	ZnO@ZIF-8	0.0391	0.0951	0.0673
9	ZIF-L	0.1450	0.1799	0.0680
10	ZnO@ZIF-L	0.2500	1.7507	0.7829

The lowest concentration of ZnO@ZIF-8 with the ability to kill *E. coli* was Sample 4 at 0.0228 mg mL<sup>-1</sup>, derived from calcined ZIF-8 prepared using methanol. This sample also presented the lowest values of standard deviation and standard error, supporting the choice to continue investigations with this sample. The lowest concentration of ZIF-8 required to kill however, was 0.0575 mg mL<sup>-1</sup>, prepared using TEA. Unfortunately, this data also presented the greatest values of standard deviation and error, though reasons for such varied results across both technical and biological repeats remains unclear. It is worth noting that this sample demonstrated a particularly strong static charge, which formed only when ZIF-8 had been synthesised using TEA. Since the mechanism by which the bacteria is killed is unknown, this observation may have relevance. The average MBC (mg mL<sup>-1</sup>) demonstrates that whilst ZIF-8 exhibited bactericidal activity, ZnO@ZIF-8 formed from its calcined ZIF-8 precursor had greater bactericidal abilities. Notably, ZIF-8 and ZnO@ZIF-8 compounds of different morphologies, showed differences in MBCs (mg mL<sup>-1</sup>). This is likely due to differences in the polarity, shape, size and surface area available for antimicrobial action. When comparing ZnO@ZIF-8 to ZIF-8 alone, the presence of ZnO nanorods explains the lowered MBC.<sup>9</sup> Based on the MBC results, ZIF-L and ZnO@ZIF-L were omitted from further studies due to the exceptionally large average values and ZnO@ZIF-L's reasonably high value of standard deviation. ZIF-8 and ZnO@ZIF-8 prepared using both organic and aqueous syntheses were carried forward for preparation of composite polymer samples and antimicrobial testing of the composite samples.

### **3.3. Silicone elastomers containing ZIF-8 and ZnO@ZIF-8**

#### **3.3.1. Effect of ZIF-8 and ZnO@ZIF-8 addition on polymer curing**

During primary trials using the manufacturer's instructions: mixing 10:1 Part A to Part B (Technovent, UK), and adding 4 wt.% ZIF sample, polymer composites failed to cure completely. Despite following both recommended cure times and conditions (room temperature and pressure for 24 hours or 1 hour at 100°C), neither method produced usable results. Issues arose with incomplete curing that resulted in the composite plaques sticking to the mould. This suggested that the MOFs were preferentially adsorbing the manufactured crosslinker and/or the Pt based catalyst.

To resolve this, an alternative method of preparation was conducted. Reactant ratios, mix times and curing conditions were adjusted. This led to increased amounts of the M511 component containing the functionalised Si polymer and Pt catalyst. PTFE sheets also replaced the original steel sandwiching sheets of the mould, in order to counter the issue of any residual tendency for the sheets to adhere to the composite samples.

### 3.3.2. Effect of adsorbed gas release on cured polymer structure

Further complications arose during trials forming composite samples, whereby tiny air bubbles could be seen throughout the entire polymer sheet. This highlighted issues regarding adsorbed gas release from the ZIF-8 incorporated. To rectify this, ZIF-8 samples were dried overnight in an oven at 100°C, prior to use. The mixing and settling of composite components was conducted under vacuum, and curing of the composite samples was operated under both heated and pressurised conditions by means of the hydraulic press. This successfully removed any immediately visible porosity, thus indicating that adsorbed water had been its major cause.

### 3.3.3. Macro-dispersion quality

Digital images illustrated the macro-dispersion, i.e. the dispersion of large agglomerates, of the ZIF structures within the cured silica matrix (**Fig. 16**).

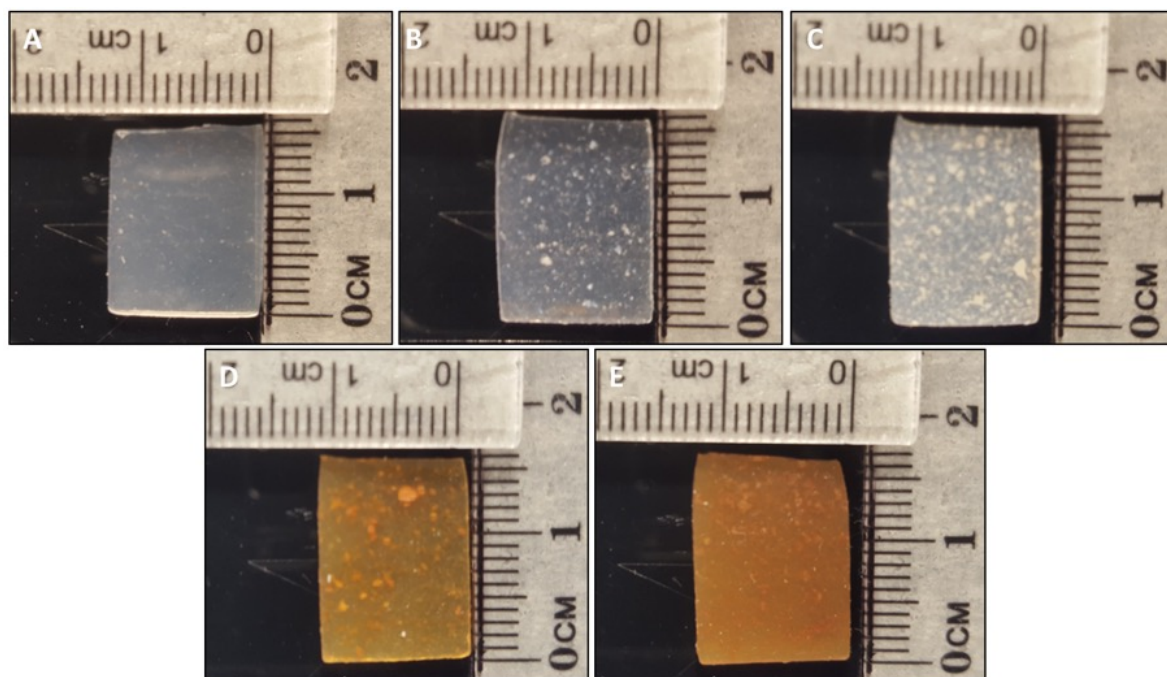


**Figure 16: Digital images of cured composite samples containing (A) unfilled matrix, (B) ZIF-8 prepared with MeOH, (C) ZnO@ZIF-8 prepared with MeOH, (D) ZIF-8 prepared with TEA and (E) ZnO@ZIF-8 prepared with TEA.**

These images display clear colour differences between cured composite samples, containing ZIFs prepared with MeOH (**Fig. 16 B and C**) and ZIFs prepared using TEA (**Fig. 16 D and E**). Whilst (**Fig. 16B**), is most closely-related in colour to the unfilled matrix (**Fig. 16A**), notable agglomerates of ZIF-8 are present. When compared to its ZnO@ZIF-8 partner (**Fig. 16C**), the composite Sample B is less milky/cloudy with fewer agglomerations. Sample C was found to be the weakest, least stiff composite, with the highest hexane extractables (described within Section 3.3.5) – this is likely due particularly poor ZIF-8 particle dispersion, as shown.

Brown discolouration of samples prepared using TEA may originate from the presence of organic materials during calcination. This is further enhanced by the presence of Ag, which is reduced during the calcination of Sample E.

It may also be deduced that ZIF-8s formed using TEA, show slightly better dispersion, however ZIF-8 agglomerates are obscured by the general haziness of

ZnO@ZIF-8 particles (**Fig. 16E**). It should be noted that ZIF-8s produced using TEA also demonstrated a strong static charge, whilst ZIF-8s produced using MeOH did not. The static charge on the former particles indicates that they have a more hydrophobic surface than the latter particles. Greater filler surface hydrophobicity can lead to weaker filler-filler interactions and effective wetting of the filler surface by the hydrophobic silicone matrix; both these factors can lead to more rapid particle dispersion and hence better dispersion quality.<sup>150, 151</sup>

### 3.3.4. Micro-dispersion quality

SEM images illustrating the micro-dispersion (the dispersion of small aggregates) of ZIFs, within freeze-fractured surfaces, are shown in **Fig. 17**. It is immediately evident that the matrix control (**Fig. 17A**) contains fumed silica - the aggregates visible are within the expected size range of 10-20 nm.<sup>152</sup>

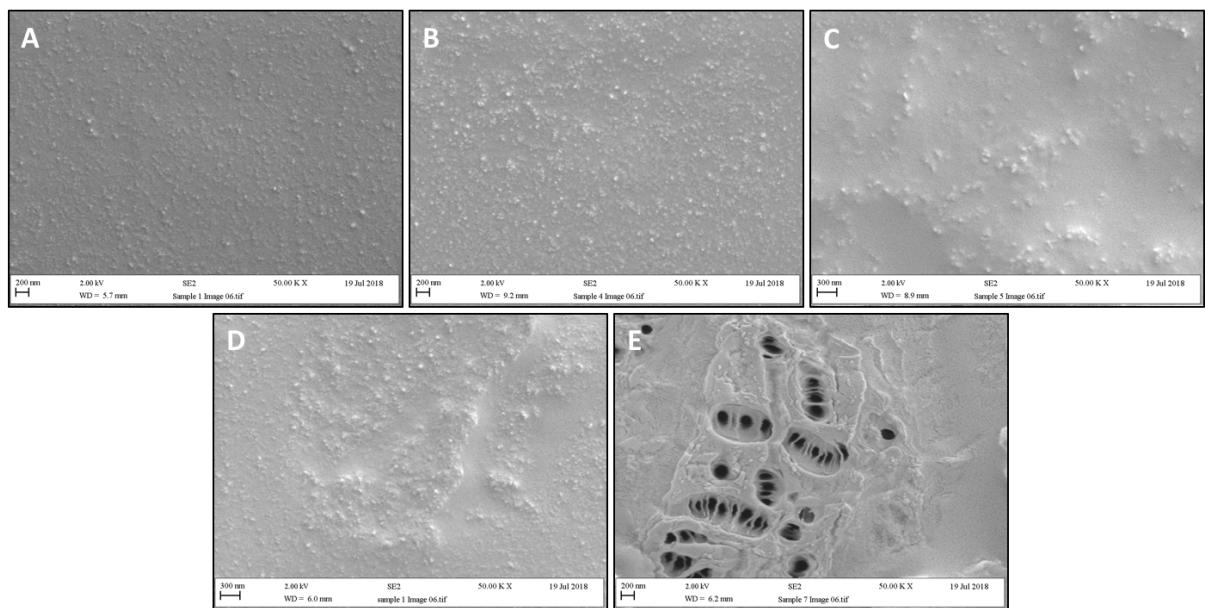


**Figure 17: SEM images of freeze-fractured composite samples containing (A) unfilled matrix, (B) ZIF-8 prepared with MeOH, (C) ZnO@ZIF-8 prepared with MeOH, (D) ZIF-8 prepared with TEA and (E) ZnO@ZIF-8 prepared with TEA. Scale bar is 200 nm (A, B and E) and 300 nm (C and D).**

These images show minor differences in the dispersion quality of ZIF-8 particles, regardless of their synthesis route. Here, the dispersion of ZIF-8 prepared using TEA (**Fig. 17D**) appears only marginally worse than that from MeOH preparation (**Fig. 17B**).

The addition of the ZnO nano-rods to the ZIF-8 seemingly worsens the micro-dispersion of ZIF-8 formed via the organic MeOH route; this is also true of the macro-dispersion in this pair of composites. Comparison of the effect of ZnO nano-rods on the dispersion of ZIF-8 particles prepared aqueously (using TEA), however, is hampered by the porosity produced (**Fig. 17E**).

### 3.3.5. Percent mass hexane swelling and extractables

Average hexane swelling (absorption) mass percentages allowed an insight into the crosslink density and filler-matrix interaction within the composites. Generally, the lower the % swelling, the greater the crosslink density and/or filler-matrix interaction (provided the majority of the chains are crosslinked into the network).

Without crosslinking, and with weak hexane displaceable filler-matrix interaction, the silicone polymer matrix would be completely soluble in hexane. In contrast, crosslinked chains are insoluble, due to the size of their network structure; solvent molecules can solvate the chains in the network (leading to the swelling effect), but due to the crosslinking between the chains, cannot take individual chains into solution.

When the interfacial area is high, and the inter-particle distance is low, very strong filler-matrix interaction occurs. This can lead to adsorption crosslinking and restricted matrix solubility, whereby a single chain may interact with more than one filler particle. As a result, entanglements could exist between loopily adsorbed chains on adjacent filler particles.

Considering experimental error, **Fig. 18A** shows that percentage mass hexane swelling levels of all composites remained similar to the unfilled matrix control. Subtle trends may be observed, however, when considering both percentage swelling and percentage extractables content; as ZIF-8, and notably ZnO@ZIF-8, prepared using MeOH, may have had slightly lower crosslink densities/ levels of filler-matrix interaction than the equivalent, aqueously synthesised samples.

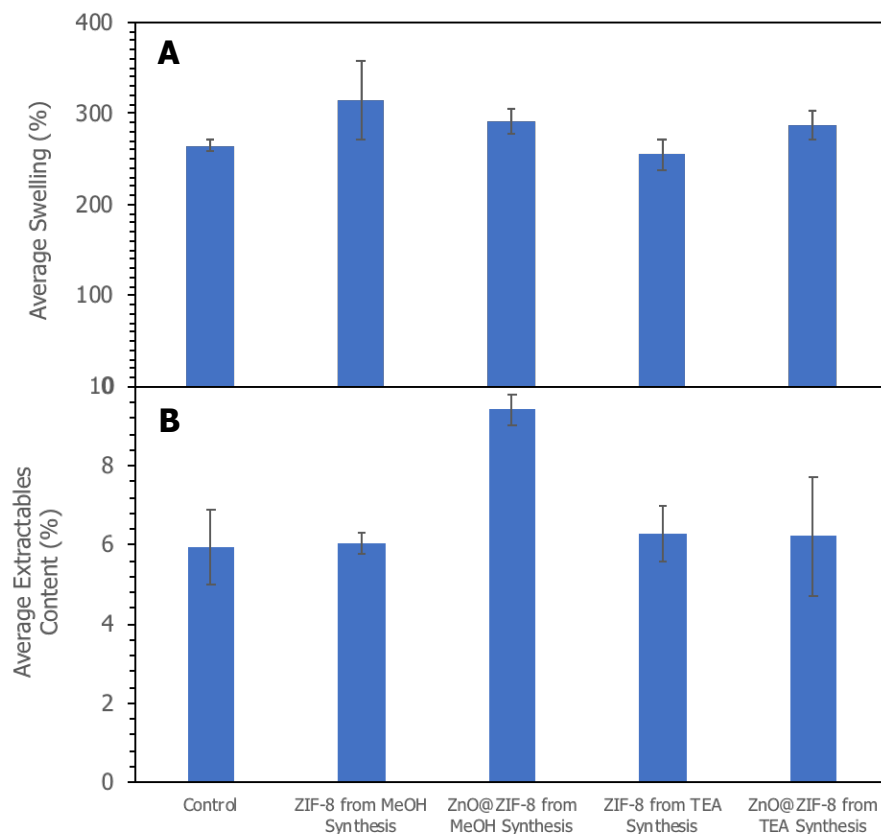


**Figure 18: Average hexane swelling (A) and extractables content (B) (all mass percentages) of ZIF samples and unfilled matrix control.**

The composite containing ZIF-8 from MeOH synthesis exhibited the largest average swelling percentage, and therefore the lowest crosslink density, indicating that this composite was likely the weakest. Nonetheless, these samples also presented the broadest standard deviation and thus, were slightly less reliable.

The average percentage swelling of samples produced using TEA (particularly containing ZIF-8), were almost identical to the unfilled control.

Average percentage masses of hexane extractables content (**Fig. 18B**) remained reasonably identical across all samples - with the exception of the organically synthesised (MeOH prepared) ZnO@ZIF-8-based composite. Though reasonably large, standard deviations of <16.500 were calculated for the other composite samples, ranging from 14.131 – 16.44. This demonstrated close consistency between the composites produced and was expectedly greater than that of the control (standard deviation of 5.801).

The organically synthesised (MeOH prepared) ZnO@ZIF-8-based composite demonstrated a 9.5% extractables content, as opposed to the average ~6% for the other samples and also housed a significantly greater standard deviation of 42.654. Reduced crosslinking within the filler-matrix interfacial region may occur if the organically synthesised ZnO@ZIF-8 particle surface, deactivates the Pt based crosslinking catalyst. Should the majority of the extractable material in this composite stem from the filler-matrix interfacial region, then the mechanical properties of this sample may become poorer.

The importance of extractables data is highlighted by **Fig. 18B**. Chains which are not chemically or strongly bonded to filler particles are extractable. This can lead to reduced levels of swelling which, in isolation, may be mistakenly interpreted as successful crosslinking, e.g. the composites formed with ZnO@ZIF-8 from MeOH synthesis. If a low level of swelling is accompanied by a high extractables content, however, then crosslinking is likely to be non-uniformly distributed in the matrix. Whilst the majority of composite samples presented similar average extractables content (%) to the unfilled matrix, percentages from those containing ZnO@ZIF-8 from MeOH synthesis were significantly higher.

### 3.3.6. Tensile testing

Average stress-strain curves for the unfilled matrix control and composite materials are shown in **Fig. 19**, with the key mechanical properties - including Young's moduli (stiffness), summarised in **Fig. 20**.

Data compiled in **Fig. 19**, supports the idea that the generally non-uniform dispersion of ZIFs within silica composites (excluding that containing organically synthesised ZnO@ZIF-8), resulted in premature failure, due to the agglomerates acting as stress concentrations/ defects. Catastrophic cracks propagated from these. Despite this, the TEA synthesised ZIF-8 showed better dispersion than those made by the MeOH route. The end of each line represents the average point of sample fracture, thus showing that the unfilled matrix was able to withstand significantly more stress and strain than each of the other composite samples. For most, this occurred at around 520% elongation with stress levels of around 2 MPa. Until this point, the composite stress-strain data remained similar to that of the unfilled matrix, though subtle variations indicated varied degrees of filler-matrix interaction.

In contrast, composites containing ZnO@ZIF-8 prepared using MeOH, produced significantly different stress-strain results. Here, the lower rate of stress increase, with increasing strain and slightly higher elongation at break, alluded to a lower crosslink density. These conditions lead to a lower Young's modulus and tensile strength. Whilst reduced crosslink density was not supported by the hexane swelling data (**Fig. 18A**), the observations can be explained by the relatively high hexane extractables content recorded for the ZnO@ZIF-8-MeOH based composite (**Fig. 18B**). The significant reduction in tensile strength and Young's modulus observed for the latter composite, indicated that the majority of extractable material had originated from the filler-matrix interfacial region.

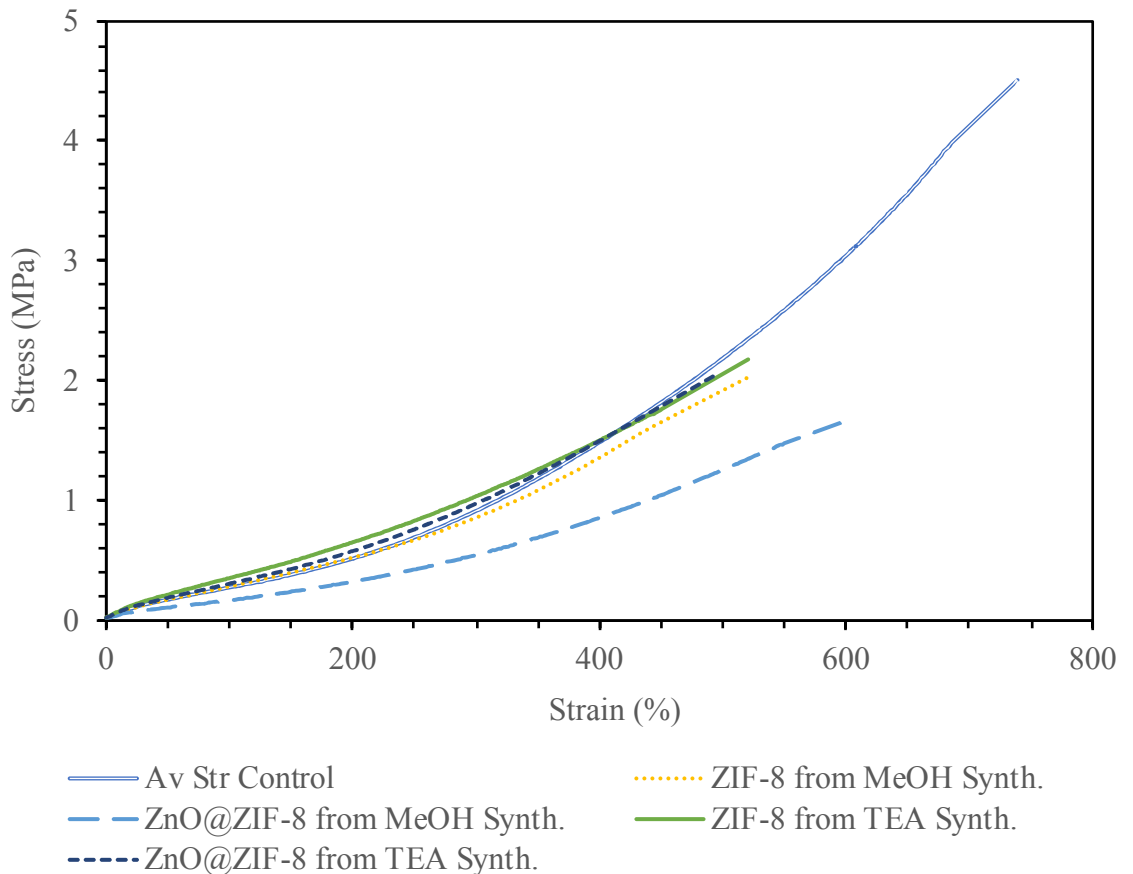


**Figure 19: Average stress-strain curves of ZIF samples versus unfilled matrix (Av Str Control).**

Experimental error considered, the Young's modulus data (**Fig. 20**) indicates that all composites (with the exception of that containing ZnO@ZIF-8 from MeOH), had broadly similar Young's moduli to the matrix control. When the data is considered alongside the filler dispersion images and the swelling data, however, corroborative trends emerge. Composites containing aqueously synthesised ZIF-8 (which used

TEA), have a Young's modulus that is generally higher than the matrix control and other ZIF-8 composites (organically synthesised using MeOH). It is likely that this TEA route, for aqueous ZIF-8 synthesis provided a more matrix-compatible, hydrophobic ZIF-8 particle surface which, in turn, resulted in better particle dispersion (**Figs. 16 and 17**) and reduced hexane swelling (**Fig. 18A**). The composite containing ZnO@ZIF-8 from MeOH had a significantly lower Young's modulus (and thus, reduced stiffness), which likely manifested from non-uniform crosslinking and potentially, substantially reduced crosslinking of the filler-matrix interfacial region. In short, curing had not properly occurred, as supported by the extractables content data.

Focusing on the elastic region of the average stress-strain curves shows the data collected more clearly. The percentage strain of each composite differs. Samples containing ZIFs synthesised from TEA show the steepest curves, indicating higher Young's moduli - exceeding that of the unfilled matrix. When relating this to the average swelling percentages and extractables content (%) in **Fig. 18**, a stiffening effect due to increased filler-matrix interaction is confirmed. ZnO@ZIF-8 from MeOH synthesis, reduces the level of filler-matrix interaction and/or the dispersion quality, as demonstrated by the noticeably less steep stress-strain curve.

From **Fig. 20** it can be concluded that composites containing ZIFs may be arranged in the following order, from best/ strongest to worst/ weakest: ZIF-8 from TEA synthesis, ZnO@ZIF-8 from TEA synthesis, ZIF-8 from MeOH synthesis then ZnO@ZIF-8 from MeOH synthesis.

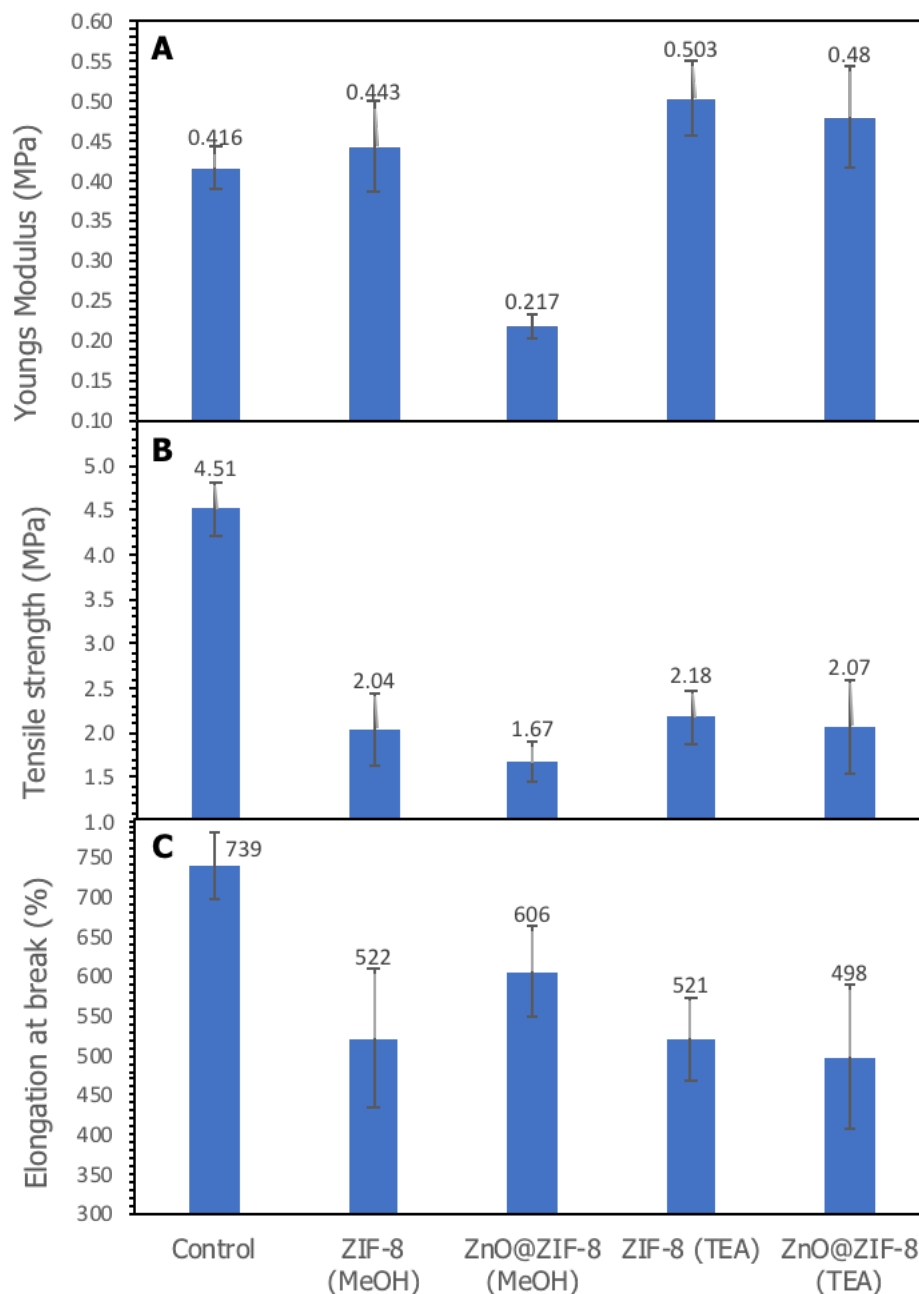


**Figure 20: Average percentage elongation at break (A), tensile strength /MPa (B) and Young's modulus /MPa (C) values of ZIF samples versus unfilled matrix control.**

Similarly, the average swelling percentage and extractables content (%), the elongation at break and the Young's modulus, gives information regarding crosslinking and filler-matrix interaction. Standard deviation error bars for each of the charts are relatively large, thus decreasing reliability of the data shown.

Relative to the unfilled matrix, the addition of all ZIFs had little effect on the Young's moduli of samples, except when ZnO@ZIF-8 from MeOH synthesis was incorporated. Standard deviation values regarding the Young's moduli ranged from

0.016 (ZnO@ZIF-8 from MeOH) to 0.064 (ZnO@ZIF-8 from TEA). Each sample, aside from that containing ZnO@ZIF-8 from MeOH, displayed a greater standard deviation than that of the control (0.027). For all composite samples, the tensile strength of the material is significantly reduced in comparison to the unfilled matrix, likely due to aggregates and/ or air pockets present throughout each composite sample. These uneven aggregates and air pockets are also responsible for such varied and large standard deviation values. This is supported by the data obtained, which depicts the elongation at break (%) displaying the largest standard deviation (89.9) upon the most air pocketed and aggregated sample (ZnO@ZIF-8 from TEA). The standard deviation of this is almost twice that of the control (41.48).

### **3.4. Antimicrobial Testing of Composite Samples**

Although reviewed and confirmed by the International Organisation for Standardization (ISO) in 2016, concerns have been raised surrounding the efficacy of BS ISO 22196:2011 when reflecting environmentally accurate conditions.<sup>153, 154</sup> The need for a better antimicrobial testing method for plastics and other non-porous surfaces remains, and analysis of the literature fails to deliver a more suitable alternative.<sup>153, 154</sup> When considering the urine flow of a catheterised patient, variations in volume and output depend upon patient fluid status and renal function.<sup>155, 156</sup> Humidity and temperature conditions of the closed environment of urinary catheterisation remains similar to protocol, however inoculation of patient urine on the polymer surface would be more frequent in practice, as the patient's bladder is constantly relieved.

#### **3.4.1. Measurement of antibacterial activity on composite samples**

Antibacterial results are shown in **Fig. 21**. As expected, coupons of the unfilled matrix displayed no antimicrobial activity, depicted by the increase of CFUs over incubated time. For each of the 4 wt.% ZIF composite samples however, bactericidal action was shown. Least effective was the composite coupons containing ZIF-8, aqueously prepared using TEA. The numbers of recoverable bacteria decreased from 0-8 hours, but then remained static up to 24 hours. This indicated that ZIF-8 was no longer actively killing the *E. coli*.

In comparison, composite coupons containing organically prepared ZIF-8 (from MeOH), showed significant biocidal activity after 3 hours incubation. At this point, a

significant decrease of 99.9% (from  $10^5$  to  $10^2$  CFU/mL) recovered bacteria was shown from T0. Following 8 hours, no organisms were recovered, up to T24. Due to this, ZIF-8 prepared using MeOH, was noted to be significantly better for biocidal use within a silicone composite. Both forms of ZnO@ZIF-8 composite coupons demonstrated the complete and retained kill of *E. coli* following 3 hours. Once the logarithms of the mean CFUs were calculated, differences between those at 0 hours were not greatly significant. These were 4.375, 4.801, 4.653, 4.336 and 4.365, with regards to the control, ZIF-8 from MeOH synthesis, ZnO@ZIF-8 from MeOH synthesis, ZIF-8 from TEA synthesis and ZnO@ZIF-8 from TEA synthesis groups, respectively. As such, the greatest difference between these values was 10.18%. Furthermore, logarithms of the standard deviations of each group indicated overlaps for each mean CFU value. These were 3.535, 4.380, 4.167, 3.713 and 3.625, in the respective order stated above. Despite incubation for 24 hours, the control group showed only an approximate 1 log increase. This may be due to a limited nutrient source, as the aliquot of LB broth was not replenished throughout incubation. Overall, ZnO@ZIF-8 composites demonstrated significant antimicrobial properties against *E. coli*, when compared to their precursor ZIF-8 composites. This was in agreement with results found by previous studies.<sup>9</sup> Using these materials in the development of urinary catheters would reduce the likelihood of biofilm formation, since cells would be unable to survive on the catheter surface.

### CFU/mL vs. Time/hour ZIF Samples vs. Control

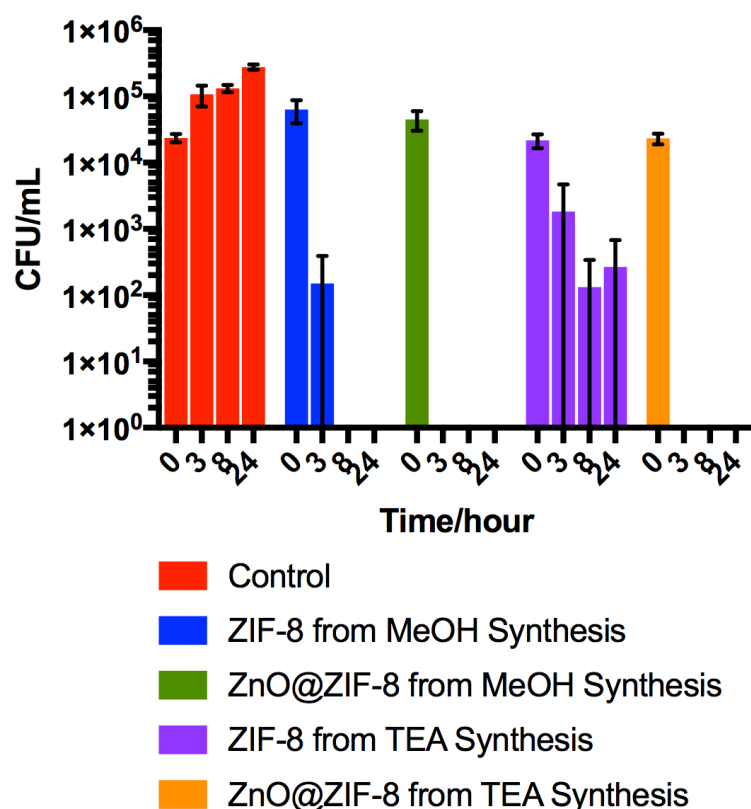


**Figure 21: Average numbers of colony forming units (living *E. coli*, CFU/mL) recovered from 4 wt.% ZIF composite coupons and unfilled matrix (control), at set time points.**

### 3.5. Metal release testing in artificial urine

Leaching of Zn and Ag from the composite samples into artificial urine, was investigated following 85 days incubation. Data presented in **Table 5** was obtained. These results are likely similar to those expected from any leaching into the microbiological testing media (LB broth), as neither solutions contain metals detrimental to the Zn of the ZIF-8 structure, and both are vastly made up of water. The highest concentration of Zn present resulted from the composite containing ZnO@ZIF-8, prepared using MeOH. This averaged at 302.73 ppb (0.30 ppm), though no reference could be found in the literature to establish whether or not this was enough to cause antimicrobial effects. However, composites containing ZnO@ZIF-8 prepared using TEA, demonstrated average concentrations of 144.05 ppb (0.14 ppm) Ag, in agreement with EDX results (**Fig. 13**). As reported by Swathy et al., Ag<sup>+</sup> released continuously from silver nanoparticles (confined in nanoscale cages) can cause antimicrobial activity in concentrations as low as 50 ppb, in

water.<sup>157</sup> Antimicrobial actions of these composites must therefore be viewed cautiously, as antimicrobial effects of Ag are now well documented.<sup>158-160</sup>

**Table 5: Concentrations of Zn and Ag detected from ICP analysis of artificial urine, following exposure to composite samples with 85 days incubation.**

Sample within Composite	Average concentration (ppb)	
	Zn	Ag
Unfilled matrix	61.43	1.13
ZIF-8 prepared using MeOH	196.53	0.44
ZIF-8 prepared using TEA	151.89	0.63
ZnO@ZIF-8 prepared using MeOH	302.73	2.54
ZnO@ZIF-8 prepared using TEA	79.56	144.05

Similarly, **Table 6** presents the average leaching concentrations of Zn and Ag from crystalline powder samples, corresponding to those embedded within the silicone elastomers. Elevated concentrations of both Zn and Ag were detected from all samples compared to results shown in **Table 5**. Most notably, ZIF-8 prepared using MeOH, presented the greatest average Zn concentration of 2368.88 ppb (2.37 ppm), thus suggesting significant leaching of Zn from the ZIF structure, however ZIF-8 prepared using TEA also showed a large increase in average concentration. Despite this, average concentrations of Zn present for samples of ZIF-8 formed using TEA and ZnO@ZIF-8 from either synthesis route appeared to release similar quantities of Zn. Furthermore, ZnO@ZIF-8 prepared via both synthesis routes appeared to leach Ag indicating that some residual Ag, which was not detected by EDX, was present within the ZnO@ZIF-8 (MeOH) sample as well. The leaching experiments show that: (i) the ZIF-8 (TEA) samples showed higher stability towards Zn leaching compared to ZIF-8 (MeOH) samples; (ii) this stability was higher for ZnO@ZIF-8 samples compared to ZIF-8 samples; (iii) silicone elastomers further reduced metal leaching from the ZIF-8 samples; and (iv) negligible concentrations of Ag were detected from ZnO@ZIF-8 (MeOH)-embedded silicone elastomers, whereas higher Ag concentrations were released from the ZnO@ZIF-8 (TEA) composite, which contributed to its antibacterial activity.

**Table 6: Concentrations of Zn and Ag detected from ICP analysis of artificial urine, following exposure to powdered samples with 85 days incubation.**

Powdered Samples	Average concentration (ppb)	
	Zn	Ag
ZIF-8 prepared using MeOH	2368.88	71.21
ZIF-8 prepared using TEA	973.70	42.66
ZnO@ZIF-8 prepared using MeOH	800.54	2465.29
ZnO@ZIF-8 prepared using TEA	954.46	7056.00

These findings were supported by the EDX data presented in **Fig. 13**, though lack of Ag depicted by **Fig. 12** is likely due to Ag's concentration being below the detection limit of EDX. It is not exactly known why Ag is present in the ZIF-8 samples, as it is not an expected impurity in the zinc salts used in preparation. Such small amounts may have been detected following contamination of the ICP-MS equipment, or from the vials and apparatus used. The levels reported are very close to, and below, those known to exhibit any antimicrobial activity.<sup>157</sup> Since Ag is not a component in the ZIF-8 framework, it is unlikely that a continuous release of Ag<sup>+</sup> is present, and so only negligible effects on antimicrobial ability could occur, over time. For ZnO@ZIF-8 samples however, some amounts of Ag were expected as residue from silver nitrate treatment.

XRD was further used to study the degree of framework's stability after the leaching experiments. XRD patterns of ZIF-8 prepared using MeOH showed structural differences between the sample, pre and post incubation within artificial urine. This suggested that the ZIF-8 framework had partially collapsed and that another crystalline material had formed, thus explaining the increased average concentrations of Zn reported by ICP analysis (**Fig. 22**). Additional peaks were also detected on the ZnO@ZIF-8 (MeOH) samples, although the main crystalline phase was still ZIF-8 (**Fig. 23**). This result confirms the ICP results that the post-synthesis treatment with silver nitrate stabilised the ZIF-8 structure.

The significant antimicrobial properties of ZnO@ZIF-8, shown by data presented in **Fig. 21**, are likely related to the leaching of Zn and Ag ions present. The higher the

bactericidal activity of ZIF-8 (MeOH) could be explained by the higher amounts of the Zn leached. Furthermore, the highest activity of the ZnO@ZIF-8 (TEA) may be due to the release of Ag from the composite.

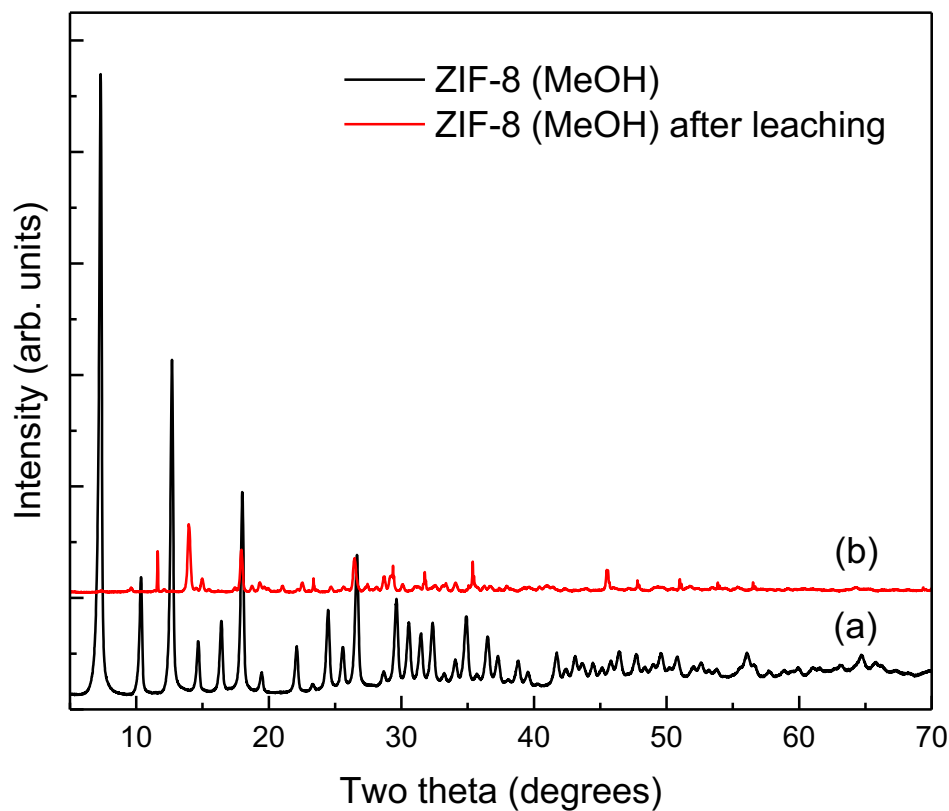


**Figure 22: XRD patterns of the batch ZIF-8 sample prepared from the MeOH system: (a) before and (b) after leaching.**

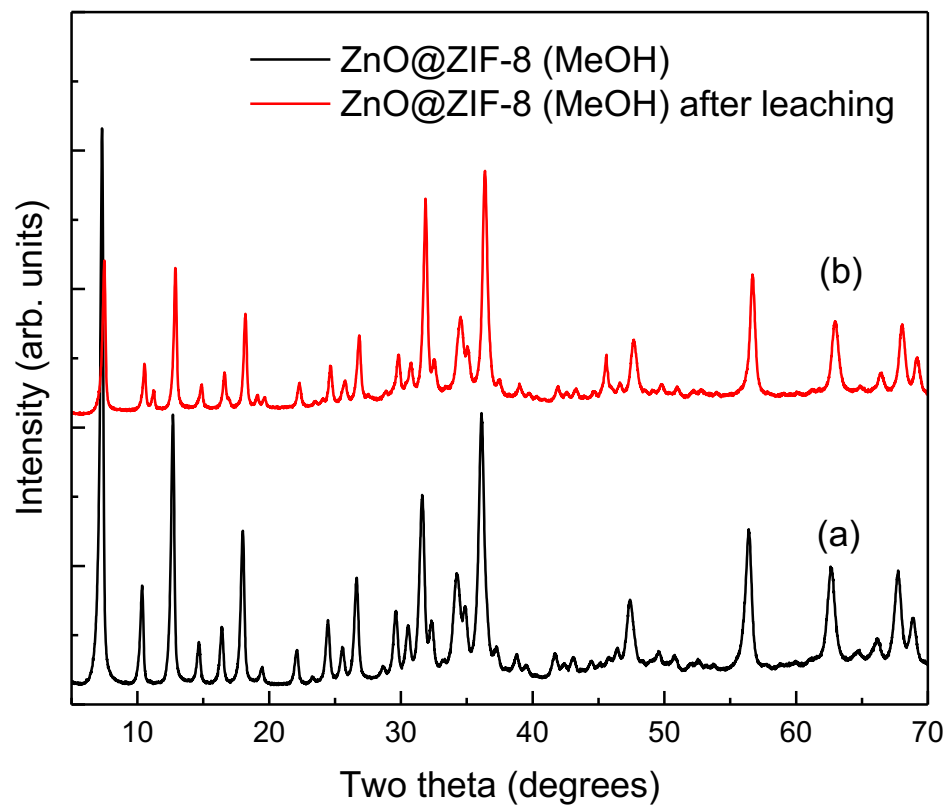


**Figure 23: XRD patterns of the batch ZnO@ZIF-8 sample prepared from the MeOH system: (a) before and (b) after leaching.**

**Figs. 24 and 25** showed that the ZIF-8 (TEA) samples retained their structure after incubation in artificial urine, although a certain decrease in the intensity of the XRD peaks was detected following leaching.

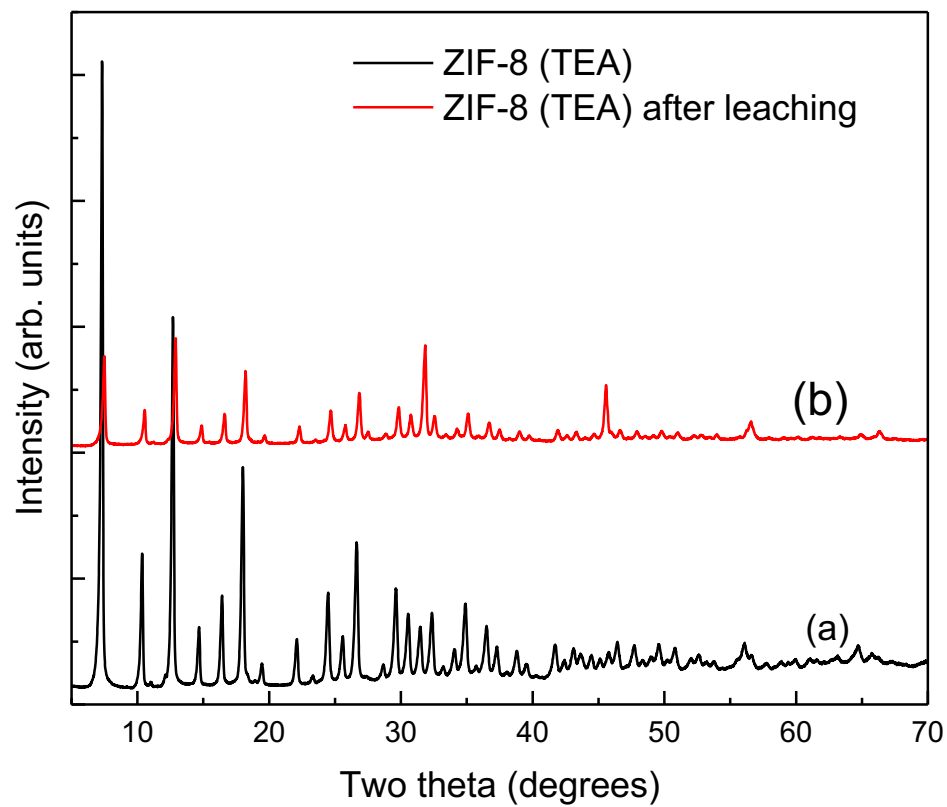


**Figure 24: XRD patterns of the batch ZIF-8 sample prepared from the TEA system: (a) before and (b) after leaching.**

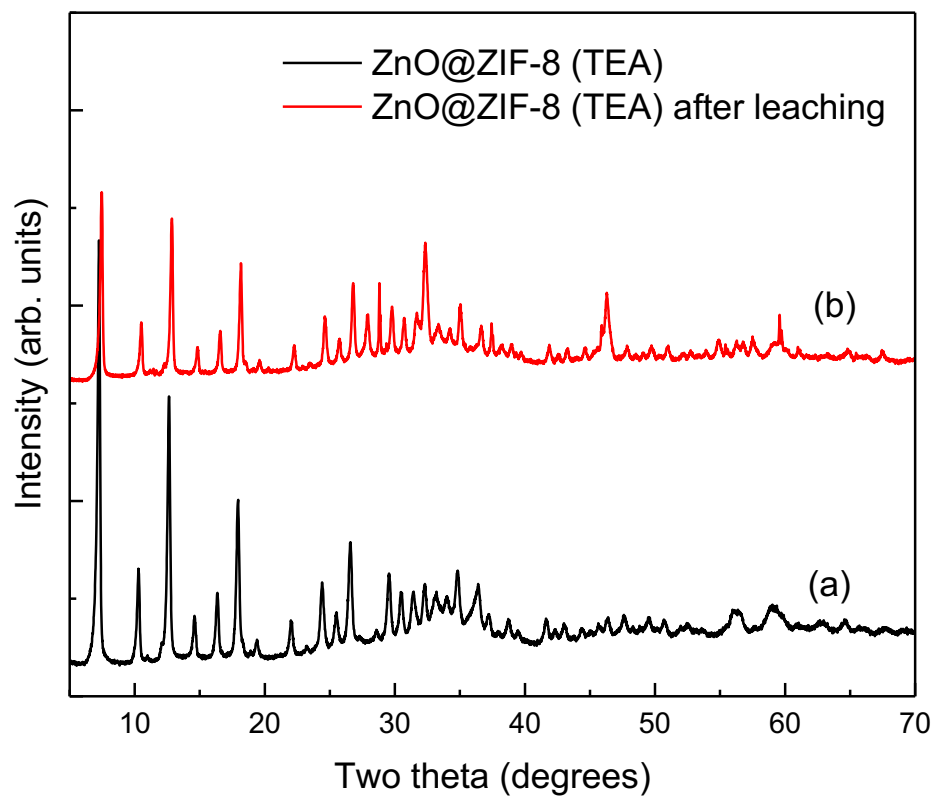


**Figure 25: XRD patterns of the batch ZnO@ZIF-8 sample prepared from the TEA system: (a) before and (b) after leaching.**

## CHAPTER 4: CONCLUSIONS

This project investigated the further development of novel biocide-containing silicones for potential use in urinary catheters, for the control of microbial colonisation. ZIF-8 and ZnO@ZIF-8 were studied as potential antibacterial agents, against the model bacterium *E. coli*, with various synthesis routes considered. These included both organic and aqueous methods, resulting in crystal formations with differing particle sizes. It was identified that whilst the synthesis route, organic or aqueous, had a pioneering effect on the antibacterial activity, the addition of ZnO nanorods significantly increased the biocidal abilities of ZIF-8. This supported existing literature, which described the efficacy of ZnO@ZIF-8 in relation to nanocrystalline ZnO alone.<sup>9</sup> The relationship between the ZIF-8's synthesis route and antibacterial activity has not yet been discussed in existing literature, though varied mechanisms for ZIF-8's antibacterial action have been suggested.<sup>8, 56, 161</sup> Whilst it is broadly accepted that ZnO possesses antimicrobial abilities, and that nanoparticles offer greater efficacies with regards to their microparticle counterparts, incorporating bactericidal components with MOFs remains in its infancy.<sup>128, 133, 161, 162</sup>

Incorporation of the ZIFs to form silicone composites was achieved, with most physical properties remaining relatively similar to those of the unfilled silicone matrix, commonly used in biomedical applications today. The curing of silicone elastomers in this study, required altered components and conditions when compared to those described by Redfern et al.<sup>9</sup> This may be due to slight differences in the ZIF-8 formed via different syntheses, since this study describes noticeable variations observed between each silicone elastomer formed.

Leaching studies revealed the potential breakdown of the ZIF-8 framework depending upon its synthesis route, which released Zn<sup>2+</sup> ions into the solution. Since these are notably antimicrobial, different biocidal mechanisms may depend upon the ZIF-8's stability, and in turn, its route of formation.

## CHAPTER 5: FUTURE WORK

Results and limitations highlighted by this study indicated the following areas as recommendations for further work:

### *Chemical investigations*

- ZIFs of other morphologies may be considered for the tests examined above. This may include the use of sodium formate and/or n-Butylamine for ZIF-8 formation, as demonstrated by Cravillon et al. Here, an excess of the bidentate ligand and various simple auxiliary monodentate ligands, with different chemical functionalities (e.g. carboxylate, N-heterocycle, alkylamine) are applied to control/ alter the crystal size.<sup>163</sup>
- Further analysis of leaching tests may be conducted to investigate whether any harmful by-products are made due to the interactions of urine and the MOF over time, particularly if the MOF is gradually degrading. BET analysis of the samples post-leaching would also highlight changes to the ZIFs' surface areas following prolonged urine exposure. EDX analysis of the recovered, dried powders would also provide compositional information.
- Methods described in this project could be used for further leaching tests, to examine any differences between leaching in artificial urine and leaching in LB broth.
- Analysis of the composite samples post-urine exposure may also indicate whether or not salt crystals would form from surface interactions, thus highlighting potential issues regarding catheter blockages and encrustation.
- A physical mixture of ZnO nanorods and ZIF-8 should be tested by the same means of this study, to conclude whether or not this could be a potential candidate for the formation of an antibacterial composite. Since previous studies highlight the antibacterial ability of ZnO nanocrystals (<100nm) alone, and this study highlights the antimicrobial abilities of ZIF-8 (alone and alongside ZnO@ZIF-8), this would be a plausible inquiry.<sup>9</sup>

### *Microbiological investigations*

- Other CAUTI-associated pathogens such as *Klebsiella pneumoniae*, *Proteus mirabilis*, *Enterobacter cloacae* and *Staphylococcus aureus* should be investigated.
- Further tests, to collate evidence regarding bacterial interaction on the composite surface, such as adhesion assays, crude viability testing, and/or 24 hour and 48 hour biofilm testing should be conducted.
- Alternatives or adaptations to BS ISO 22196:2011 should be considered to enhance the relevance of experimental results to those expected *in vivo*, e.g. composites should be exposed to a continuous drip of live culture, simulating the frequent/ continuous exposure of the material to bacteria and urine, in catheterised patients.
- Further investigations must be conducted in order to investigate the mechanism by which antibacterial activity occurs.
- Since composites may ultimately come into contact with natural barriers, e.g. the urethral epithelium, further investigations must be conducted into how the MOF nanoparticles may interact.
- Furthermore, toxicity studies of ZIF-8 and ZnO@ZIF-8 must be conducted, despite current evidence showing unharmed characteristics in similar MOF structures.<sup>164</sup>

## REFERENCES

1. P. A. Tambyah and J. Oon, *Current opinion in infectious diseases*, 2012, **25**, 365-370.
2. P. Zarb, B. Coignard, J. Griskeviciene, A. Muller, V. Vankerckhoven and H. Goossens, *EuroSurveillance Monthly*, 2012, **17**, 20316.
3. D. Stickler, R. Young, G. Jones, N. Sabbuba and N. Morris, *Urological research*, 2003, **31**, 306-311.
4. D. J. Stickler, *Nature Reviews Urology*, 2008, **5**, 598.
5. D. Stickler and J. Zimakoff, *Journal of Hospital Infection*, 1994, **28**, 177-194.
6. L. E. Nicolle, *Antimicrobial resistance and infection control*, 2014, **3**, 23.
7. A. C. McKinlay, R. E. Morris, P. Horcajada, G. Férey, R. Gref, P. Couvreur and C. Serre, *Angewandte Chemie International Edition*, 2010, **49**, 6260-6266.
8. G. Wyszogrodzka, B. Marszałek, B. Gil and P. Dorożyński, *Drug Discovery Today*, 2016, **21**, 1009-1018.
9. J. Redfern, L. Geerts, J. W. Seo, J. Verran, L. Tosheva and L. H. Wee, *ACS Applied Nano Materials*, 2018, **1**, 1657-1665.
10. O. K. Farha, I. Eryazici, N. C. Jeong, B. G. Hauser, C. E. Wilmer, A. A. Sarjeant, R. Q. Snurr, S. T. Nguyen, A. O. Z. R. Yazaydin and J. T. Hupp, *Journal of the American Chemical Society*, 2012, **134**, 15016-15021.
11. S. Wang, C. M. McGuirk, A. d'Aquino, J. A. Mason and C. A. Mirkin, *Advanced Materials*, 2018, **30**, 180-202.
12. H.-C. Zhou, J. R. Long and O. M. Yaghi, *Chem. Rev.*, 2012, **112**, 673-674.
13. B. F. Hoskins and R. Robson, *Journal of the American Chemical Society*, 1989, **111**, 5962-5964.
14. O. M. Yaghi, G. Li and H. Li, *Nature*, 1995, **378**, 703-706.
15. O. M. Yaghi and H. Li, *J. Am. Chem. Soc.*, 1995, **117**, 10401-10402.
16. D. Farrusseng, S. Aguado and C. Pinel, *Angewandte Chemie International Edition*, 2009, **48**, 7502-7513.
17. T. L. Easun, F. Moreau, Y. Yan, S. Yang and M. Schröder, *Chemical Society Reviews*, 2017, **46**, 239-274.
18. A. J. Howarth, Y. Liu, P. Li, Z. Li, T. C. Wang, J. T. Hupp and O. K. Farha, *Nature Reviews Materials*, 2016, **1**, 15018.
19. W. Lin, W. J. Rieter and K. M. Taylor, *Angewandte Chemie International Edition*, 2009, **48**, 650-658.
20. N. Rangnekar, N. Mittal, B. Elyassi, J. Caro and M. Tsapatsis, *Chemical Society Reviews*, 2015, **44**, 7128-7154.
21. S. Dang, Q.-L. Zhu and Q. Xu, *Nature Reviews Materials*, 2017, **3**, 17075.
22. S. Kitagawa, R. Kitaura and S. I. Noro, *Angewandte Chemie International Edition*, 2004, **43**, 2334-2375.
23. G. Férey and C. Serre, *Chemical Society Reviews*, 2009, **38**, 1380-1399.
24. N. Stock and S. Biswas, *Chemical reviews*, 2011, **112**, 933-969.
25. Z. X. Low, J. Yao, Q. Liu, M. He, Z. Wang, A. K. Suresh, J. Bellare and H. Wang, *Crystal Growth & Design*, 2014, **14**, 6589-6598.
26. N. A. Khan and S. H. Jhung, *Coordination Chemistry Reviews*, 2015, **285**, 11-23.
27. Z. Ni and R. I. Masel, *Journal of the American Chemical Society*, 2006, **128**, 12394-12395.
28. A. Martinez Joaristi, J. Juan-Alcañiz, P. Serra-Crespo, F. Kapteijn and J. Gascon, *Crystal Growth & Design*, 2012, **12**, 3489-3498.

29. T. Friščić, D. G. Reid, I. Halasz, R. S. Stein, R. E. Dinnebier and M. J. Duer, *Angewandte Chemie*, 2010, **122**, 724-727.
30. W. J. Son, J. Kim, J. Kim and W. S. Ahn, *Chemical Communications*, 2008, **47**, 6336-6338.
31. A. Rabenau, *Angewandte Chemie International Edition in English*, 1985, **24**, 1026-1040.
32. R. E. Morris, P. S. Wheatley, S. Warrender and M. Duncan, *APL Materials*, 2018, **2**, 124108.
33. A. Pichon, A. Lazuen-Garay and S. L. James, *CrystEngComm*, 2006, **8**, 211-214.
34. J. Klinowski, F. A. A. Paz, P. Silva and J. Rocha, *Dalton Transactions*, 2011, **40**, 321-330.
35. J.-S. Choi, W.-J. Son, J. Kim and W.-S. Ahn, *Microporous and Mesoporous Materials*, 2008, **116**, 727-731.
36. T. Shono, D. Mingos, D. Baghurst and P. Lickiss, *The New Chemistry*, Cambridge University Press, Cambridge United Kingdom, 2000.
37. A. Cadiau, J. S. Lee, D. Damasceno Borges, P. Fabry, T. Devic, M. T. Wharmby, C. Martineau, D. Foucher, F. Taulelle and C. H. Jun, *Advanced Materials*, 2015, **27**, 4775-4780.
38. X. Zhao, X. Bu, T. Wu, S.-T. Zheng, L. Wang and P. Feng, *Nature Communications*, 2013, **4**, 2344.
39. J. R. Li, R. J. Kuppler and H. C. Zhou, *Chemical Society Reviews*, 2009, **38**, 1477-1504.
40. H. Wu, T. Yildirim and W. Zhou, *The journal of physical chemistry letters*, 2013, **4**, 925-930.
41. I. Stassen, N. Burtch, A. Talin, P. Falcaro, M. Allendorf and R. Ameloot, *Chemical Society Reviews*, 2017, **46**, 3185-3241.
42. R. F. Mendes and F. A. A. Paz, *Inorganic Chemistry Frontiers*, 2015, **2**, 495-509.
43. J. Liu, L. Chen, H. Cui, J. Zhang, L. Zhang and C.-Y. Su, *Chemical Society Reviews*, 2014, **43**, 6011-6061.
44. J. A. Mason, J. Oktawiec, M. K. Taylor, M. R. Hudson, J. Rodriguez, J. E. Bachman, M. I. Gonzalez, A. Cervellino, A. Guagliardi and C. M. Brown, *Nature*, 2015, **527**, 357.
45. M. Eddaoudi, J. Kim, N. Rosi, D. Vodak, J. Wachter, M. O'keeffe and O. M. Yaghi, *Science*, 2002, **295**, 469-472.
46. J. M. Holcroft, K. J. Hartlieb, P. Z. Moghadam, J. G. Bell, G. Barin, D. P. Ferris, E. D. Bloch, M. M. Algaradah, M. S. Nassar and Y. Y. Botros, *Journal of the American Chemical Society*, 2015, **137**, 5706-5719.
47. T. M. McDonald, J. A. Mason, X. Kong, E. D. Bloch, D. Gygi, A. Dani, V. Crocella, F. Giordanino, S. O. Odoh and W. S. Drisdell, *Nature*, 2015, **519**, 303.
48. N. S. Bobbitt, M. L. Mendonca, A. J. Howarth, T. Islamoglu, J. T. Hupp, O. K. Farha and R. Q. Snurr, *Chemical Society Reviews*, 2017, **46**, 3357-3385.
49. E. Barea, C. Montoro and J. A. Navarro, *Chemical Society Reviews*, 2014, **43**, 5419-5430.
50. T. Faust, *Nature Chemistry*, 2015, **7**, 270.
51. C. Orellana-Tavra, E. F. Baxter, T. Tian, T. D. Bennett, N. K. Slater, A. K. Cheetham and D. Fairen-Jimenez, *Chemical Communications*, 2015, **51**, 13878-13881.
52. P. Li, J. A. Modica, A. J. Howarth, E. Vargas, P. Z. Moghadam, R. Q. Snurr, M. Mrksich, J. T. Hupp and O. K. Farha, *Chem*, 2016, **1**, 154-169.
53. P. Horcajada, R. Gref, T. Baati, P. K. Allan, G. Maurin, P. Couvreur, G. Ferey, R. E. Morris and C. Serre, *Chemical reviews*, 2011, **112**, 1232-1268.
54. R. E. Morris and L. Brammer, *Chemical Society Reviews*, 2017, **46**, 5444-5462.

55. J. C. AP Co<sup>^</sup>te, R. Huang, F. J. Uribe-Romo, H. K. Chae, M. O'Keeffe and O. M. Yaghi, *Proc. Natl. Acad. Sci. USA*, 2006, **103**, 10186-10191.
56. H. Nabipour, M. H. Sadr and G. R. Bardajee, *New Journal of Chemistry*, 2017, **41**, 7364-7370.
57. K. Zhou, B. Mousavi, Z. Luo, S. Phatanasri, S. Chaemchuen and F. Verpoort, *Journal of Materials Chemistry A*, 2017, **5**, 952-957.
58. S. Conrad, P. Kumar, F. Xue, L. Ren, S. Henning, C. Xiao, K. A. Mkhoyan and M. Tsapatsis, *Angewandte Chemie International Edition*, 2018, **57**, 41.
59. I. U. Khan, M. H. D. Othman, A. Ismail, N. Ismail, J. Jaafar, H. Hashim, M. A. Rahman and A. Jilani, *Materials Characterization*, 2018, **136**, 407-416.
60. K. S. Park, Z. Ni, A. P. Côté, J. Y. Choi, R. Huang, F. J. Uribe-Romo, H. K. Chae, M. O'Keeffe and O. M. Yaghi, *Proceedings of the National Academy of Sciences*, 2006, **103**, 10186-10191.
61. T. Pham, K. A. Forrest, H. Furukawa, J. Eckert and B. Space, *The Journal of Physical Chemistry C*, 2018, **122**, 15435-15445.
62. A. Phan, C. J. Doonan, F. J. Uribe-Romo, C. B. Knobler, M. O'keeffe and O. M. Yaghi, *Acc. Chem. Res*, 2010, **43**, 58-67.
63. K. Eum, K. C. Jayachandrababu, F. Rashidi, K. Zhang, J. Leisen, S. Graham, R. P. Lively, R. R. Chance, D. S. Sholl and C. W. Jones, *Journal of the American Chemical Society*, 2015, **137**, 4191-4197.
64. S. Bhattacharyya, R. Han, W.-G. Kim, Y. Chiang, K. C. Jayachandrababu, J. T. Hungerford, M. R. Dutzer, C. Ma, K. S. Walton and D. S. Sholl, *Chemistry of Materials*, 2018, **30**, 4089-4101.
65. X. Ma, P. Kumar, N. Mittal, A. Khlyustova, P. Daoutidis, K. A. Mkhoyan and M. Tsapatsis, *Science*, 2018, **361**, 1008-1011.
66. T. D. Bennett, A. L. Goodwin, M. T. Dove, D. A. Keen, M. G. Tucker, E. R. Barney, A. K. Soper, E. G. Bithell, J.-C. Tan and A. K. Cheetham, *Physical review letters*, 2010, **104**, 115503.
67. K. W. Chapman, G. J. Halder and P. J. Chupas, *Journal of the American Chemical Society*, 2009, **131**, 17546-17547.
68. T. D. Bennett and A. K. Cheetham, *Accounts of chemical research*, 2014, **47**, 1555-1562.
69. Y. Zhou and C.-j. Liu, *Plasma Chemistry and Plasma Processing*, 2011, **31**, 499-506.
70. M. R. Ryder, Z. Zeng, K. Titov, Y. Sun, E. Mahdi, I. Flyagina, T. D. Bennett, B. Civalieri, C. S. Kelley and M. D. Frogley, *The journal of physical chemistry letters*, 2018, **9**, 2678-2684.
71. J. C. Tan, T. D. Bennett and A. K. Cheetham, *Proceedings of the National Academy of Sciences*, 2010, **107**, 9938-9943.
72. K. Park and Z. Ni, *Proc. Natl. Acad. Sci. USA*, 2006, **103**, 10186-10191.
73. C. Zhang, R. P. Lively, K. Zhang, J. R. Johnson, O. Karvan and W. J. Koros, *The journal of physical chemistry letters*, 2012, **3**, 2130-2134.
74. Y. Pan and Z. Lai, *Chemical Communications*, 2011, **47**, 10275-10277.
75. M. C. McCarthy, V. Varela-Guerrero, G. V. Barnett and H.-K. Jeong, *Langmuir*, 2010, **26**, 14636-14641.
76. Y. Pan, B. Wang and Z. Lai, *Journal of membrane science*, 2012, **421**, 292-298.
77. R. Anderson, B. Schweitzer, T. Wu, M. A. Carreon and D. A. Gomez-Gualdrón, *ACS applied materials & interfaces*, 2017, **10**, 582-592.
78. H. N. Abdelhamid, Z. Huang, A. M. El-Zohry, H. Zheng and X. Zou, *Inorganic chemistry*, 2017, **56**, 9139-9146.
79. S. Li, K. Wang, Y. Shi, Y. Cui, B. Chen, B. He, W. Dai, H. Zhang, X. Wang and C. Zhong, *Advanced Functional Materials*, 2016, **26**, 2715-2727.

80. H. Hayashi, A. P. Cote, H. Furukawa, M. O'Keefe and O. M. Yaghi, *Nature materials*, 2007, **6**, 501.
81. G. Zhao, H. Wu, R. Feng, D. Wang, P. Xu, H. Wang, Z. Guo and Q. Chen, *ACS Omega*, 2018, **3**, 9790-9797.
82. K. Schlichte, T. Kratzke and S. Kaskel, *Microporous and Mesoporous Materials*, 2004, **73**, 81-88.
83. L. Wen, D. e. Wang, C. Wang, F. Wang, D. Li and K. Deng, *Journal of Solid State Chemistry*, 2009, **182**, 574-579.
84. Y. Pan, Y. Liu, G. Zeng, L. Zhao and Z. Lai, *Chemical Communications*, 2011, **47**, 2071-2073.
85. A. F. Gross, E. Sherman and J. J. Vajo, *Dalton transactions*, 2012, **41**, 5458-5460.
86. S. Tanaka, K. Kida, M. Okita, Y. Ito and Y. Miyake, *Chemistry Letters*, 2012, **41**, 1337-1339.
87. N. Nordin, A. Ismail, A. Mustafa, P. Goh, D. Rana and T. Matsuura, *RSC Advances*, 2014, **4**, 33292-33300.
88. I. Stassen, M. Styles, G. Greci, H. Van Gorp, W. Vanderlinden, S. De Feyter, P. Falcaro, D. De Vos, P. Vereecken and R. Ameloot, *Nature materials*, 2016, **15**, 304.
89. Q. Shi, Z. Chen, Z. Song, J. Li and J. Dong, *Angewandte Chemie*, 2011, **123**, 698-701.
90. J. Cravillon, S. Münzer, S. J. Lohmeier, A. Feldhoff, K. Huber and M. Wiebcke, *Chemistry of Materials*, 2009, **21**, 1410-1412.
91. O. Karagiari, W. Bury, J. E. Mondloch, J. T. Hupp and O. K. Farha, *Angewandte Chemie International Edition*, 2014, **53**, 4530-4540.
92. P. Deria, J. E. Mondloch, E. Tylianakis, P. Ghosh, W. Bury, R. Q. Snurr, J. T. Hupp and O. K. Farha, *Journal of the American Chemical Society*, 2013, **135**, 16801-16804.
93. P. Deria, W. Bury, J. T. Hupp and O. K. Farha, *Chemical Communications*, 2014, **50**, 1965-1968.
94. Z. Zhang, S. Xian, Q. Xia, H. Wang, Z. Li and J. Li, *AIChE Journal*, 2013, **59**, 2195-2206.
95. L. H. Wee, N. Janssens, S. P. Sree, C. Wiktor, E. Gobechiya, R. A. Fischer, C. E. Kirschhock and J. A. Martens, *Nanoscale*, 2014, **6**, 2056-2060.
96. X. Yang, Z. Wen, Z. Wu and X. Luo, *Inorganic Chemistry Frontiers*, 2018, **5**, 687-693.
97. K. Tam, A. Djurišić, C. Chan, Y. Xi, C. Tse, Y. Leung, W. Chan, F. Leung and D. Au, *Thin solid films*, 2008, **516**, 6167-6174.
98. M. Jaisai, S. Baruah and J. Dutta, *Beilstein journal of nanotechnology*, 2012, **3**, 684-691.
99. A. Sirelkhatim, S. Mahmud, A. Seeni, N. H. M. Kaus, L. C. Ann, S. K. M. Bakhori, H. Hasan and D. Mohamad, *Nano-Micro Letters*, 2015, **7**, 219-242.
100. World Health Organization, <https://www.who.int/drugresistance/documents/surveillancereport/en/>, (accessed August 2019).
101. L. M. Durso and K. L. Cook, *Current opinion in microbiology*, 2014, **19**, 37-44.
102. R. Gustafson and R. Bowen, *Journal of applied microbiology*, 1997, **83**, 531-541.
103. T. M. File Jr, A. Srinivasan and J. G. Bartlett, *Clinical infectious diseases*, 2014, **59**, 593-596.
104. P. Courvalin, *Journal of internal medicine*, 2008, **264**, 4-16.
105. J. O'Neill, *HM Government and Welcome Trust: UK*, 2018.
106. R. Smith and J. Coast, *Bmj*, 2013, **346**, 1493.
107. F. Rossi, R. Girardello, A. P. Cury, T. S. R. Di Gioia, J. N. D. Almeida Jr and A. J. D. S. Duarte, *Brazilian Journal of Infectious Diseases*, 2017, **21**, 98-101.

108. R. Pickard, T. Lam, G. MacLennan, K. Starr, M. Kilonzo, G. McPherson, K. Gillies, A. McDonald, K. Walton and B. Buckley, *The lancet*, 2012, **380**, 1927-1935.
109. C. A. Umscheid, M. D. Mitchell, J. A. Doshi, R. Agarwal, K. Williams and P. J. Brennan, *Infection Control & Hospital Epidemiology*, 2011, **32**, 101-114.
110. World Health Organization, <https://apps.who.int/iris/handle/10665/80135>, (accessed August, 2019).
111. E. Lawrence and I. Turner, *Medical engineering & physics*, 2005, **27**, 443-453.
112. L. Winson, *British Journal of Nursing*, 1997, **6**, 1229-1252.
113. M. D. K. Getliffe, *London Balliere Tindal in association with The Royal College of Nursing*, London United Kingdom, 1997.
114. R. C. Feneley, I. B. Hopley and P. N. Wells, *Journal of medical engineering & technology*, 2015, **39**, 459-470.
115. J. W. Warren, *International journal of antimicrobial agents*, 2001, **17**, 299-303.
116. R. Daifuku and W. E. Stamm, *Jama*, 1984, **252**, 2028-2030.
117. P. Tenke, B. Köves, K. Nagy, S. J. Hultgren, W. Mendling, B. Wullt, M. Grabe, F. M. Wagenlehner, M. Cek and R. Pickard, *World journal of urology*, 2012, **30**, 51-57.
118. R. P. Stark and D. G. Maki, *New England Journal of Medicine*, 1984, **311**, 560-564.
119. D. Stickler and R. Feneley, *Spinal cord*, 2010, **48**, 784.
120. P. Tenke, T. Mezei, I. Bóde and B. Köves, *European Urology Supplements*, 2017, **16**, 138-143.
121. S. A. Jacobsen, D. Stickler, H. Mobley and M. Shirtliff, *Clinical microbiology reviews*, 2008, **21**, 26-59.
122. J. R. Johnson, P. Delavari and M. Azar, *Antimicrobial agents and chemotherapy*, 1999, **43**, 2990-2995.
123. K. Schumm and T. Lam, *Cochrane Database Syst. Rev.*, 2008, **2**, CD004013.
124. N. Sabir, A. Ikram, G. Zaman, L. Satti, A. Gardezi, A. Ahmed and P. Ahmed, *American journal of infection control*, 2017, **45**, 1101-1105.
125. M. Mowbray, X. Tan, P. S. Wheatley, R. E. Morris and R. B. Weller, *Journal of Investigative Dermatology*, 2008, **128**, 352-360.
126. K.-D. Kröncke and C. V. Suschek, *Journal of Investigative Dermatology*, 2008, **128**, 258-260.
127. J. H. Shin and M. H. Schoenfisch, *Chemistry of Materials*, 2007, **20**, 239-249.
128. Akademik Veri Yonetim Sistemi, <https://avesis.yildiz.edu.tr/yayin/423d68b5-93fc-49f1-be69-5fbef7057aa5/antibacterial-and-mechanical-properties-of-pu-zif-8-nanocomposite-coated-polyester-fabric>, (accessed August 2019)
129. D. M. Eby, H. R. Luckarift and G. R. Johnson, *ACS applied materials & interfaces*, 2009, **1**, 1553-1560.
130. P. J. P. Espitia, N. d. F. F. Soares, J. S. dos Reis Coimbra, N. J. de Andrade, R. S. Cruz and E. A. A. Medeiros, *Food and Bioprocess Technology*, 2012, **5**, 1447-1464.
131. N. Padmavathy and R. Vijayaraghavan, *Science and technology of advanced materials*, 2008, **9**, 35004.
132. J. Pasquet, Y. Chevalier, J. Pelletier, E. Couval, D. Bouvier and M. A. Bolzinger, *Colloids and Surfaces A: Physicochemical and Engineering Aspects*, 2014, **457**, 263-274.
133. O. Yamamoto, *International Journal of Inorganic Materials*, 2001, **3**, 643-646.
134. L. Zhang, Y. Jiang, Y. Ding, M. Povey and D. York, *Journal of Nanoparticle Research*, 2007, **9**, 479-489.
135. Y. Zhang and Y. Yuan, *Journa of Membrane Sciencel*, 2018, **550**, 173-197.
136. A. Colas and J. Curtis, *Biomaterials science: an introduction to materials in medicine*, 2004, **2**, 80-85.

137. A. Beigbeder, M. Linares, M. Devalckenaere, P. Degée, M. Claes, D. Beljonne, R. Lazzaroni and P. Dubois, *Advanced Materials*, 2008, **20**, 1003-1007.
138. V. R. Sastri, *Plastics in medical devices: properties, requirements, and applications*, William Andrew, New York, 2<sup>nd</sup> edn., 2013.
139. V. B. Sardar, N. Rajhans, A. Pathak and T. Prabhu, 14th International Conference on Humanizing Work and Work Environment HWWE-2016, 2016.
140. W. Noll, *Chemistry and technology of silicones*, Academic Press, London, 1968.
141. T.-F. Mah, *Journal of visualized experiments: JoVE*, 2014, **83**, 50854.
142. L. Fisher, S. Ostovapour, P. Kelly, K. Whitehead, K. Cooke, E. Storgårds and J. Verran, *Biofouling*, 2014, **30**, 911-919.
143. L. B. Khan, H. M. Read, S. R. Ritchie and T. Proft, *Journal of microbiology & biology education*, 2017, **18**.
144. L. Huang, H. Wang, J. Chen, Z. Wang, J. Sun, D. Zhao and Y. Yan, *Microporous and mesoporous materials*, 2003, **58**, 105-114.
145. W. J. Rieter, K. M. Taylor, H. An, W. Lin and W. Lin, *Journal of the American Chemical Society*, 2006, **128**, 9024-9025.
146. S. Hermes, T. Witte, T. Hikov, D. Zacher, S. Bahn Müller, G. Langstein, K. Huber and R. A. Fischer, *Journal of the American Chemical Society*, 2007, **129**, 5324-5325.
147. X. C. Huang, Y. Y. Lin, J. P. Zhang and X. M. Chen, *Angewandte Chemie International Edition*, 2006, **45**, 1557-1559.
148. P. Y. Moh, Thesis, The University of Manchester, 2012.
149. A. Stanković, S. Dimitrijević and D. Uskoković, *Colloids and Surfaces B: Biointerfaces*, 2013, **102**, 21-28.
150. J. V. Milewski and H. S. Katz, *Handbook of fillers and reinforcements for plastics*, Van Nostrand Reinhold Company, New York, 1978.
151. R. Rothon, *Particulate-filled polymer composites*, iSmithers Rapra Publishing, OH USA, 2003.
152. H. Barthel, M. Heinemann, M. Stintz and B. Wessely, *Chemical Engineering & Technology: Industrial Chemistry-Plant Equipment-Process Engineering-Biotechnology*, 1998, **21**, 745-752.
153. M. Ojeil, C. Jermann, J. Holah, S. P. Denyer and J.-Y. Maillard, *Journal of Hospital Infection*, 2013, **85**, 274-281.
154. J. Redfern, J. Tucker, L. Simmons, P. Askew, I. Stephan and J. Verran, *Methods and Protocols*, 2018, **1**, 36.
155. W. M. Fallis, *Critical care nurse*, 2005, **25**, 44-51.
156. S. Foxley, *British Journal of Nursing*, 2011, **20**, 564-569.
157. J. R. Swathy, M. U. Sankar, A. Chaudhary, S. Aigal and T. Pradeep, *Nature: Scientific Reports*, 2014, **4**, 7161.
158. S. Thomas and P. McCubbin, *Journal of wound care*, 2003, **12**, 101-107.
159. J. S. Kim, E. Kuk, K. N. Yu, J. H. Kim, S. J. Park, H. J. Lee, S. H. Kim, Y. K. Park, Y. H. Park and C.-Y. Hwang, *Nanomedicine: Nanotechnology, Biology and Medicine*, 2007, **3**, 95-101.
160. K. H. Cho, J. E. Park, T. Osaka and S. G. Park, *Electrochimica Acta*, 2005, **51**, 956-960.
161. Z. Lan, C. Wang and J. Qu, *Materials Research Bulletin*, 2019, **116**, 40-43.
162. R. Brayner, R. Ferrari-Iliou, N. Brivois, S. Djediat, M. F. Benedetti and F. Fiévet, *Nano letters*, 2006, **6**, 866-870.
163. J. Cravillon, R. Nayuk, S. Springer, A. Feldhoff, K. Huber and M. Wiebcke, *Chemistry of Materials*, 2011, **23**, 2130-2141.
164. P. Horcajada, T. Chalati, C. Serre, B. Gillet, C. Sebrie, T. Baati, J. F. Eubank, D. Heurtaux, P. Clayette and C. Kreuz, *Nature materials*, 2010, **9**, 172.

